Results in Engineering 25 (2025) 104036

Contents lists available at ScienceDirect

Results in Engineering

journal homepage: www.sciencedirect.com/journal/results-in-engineering

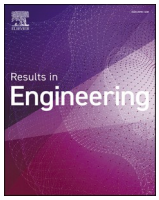

Research paper

Optimization of photocatalytic degradation of Eriochrome Black T from aqueous solution using TiO_2-biochar composite

Mohammednur Abdu [a,*], Solomon Tibebu [a], Saeideh Babaee [b], Abebe Worku [a], Titus A.M. Msagati [c], Jemal Fito Nure [b]

[a] Department of Environmental Engineering, Sustainable Energy Center of Excellence, Bioprocess and Biotechnology Center of Excellence, Nanotechnology Center of Excellence, College of Engineering, Addis Ababa Science and Technology University, 16417 Addis Ababa, Ethiopia
[b] Department of Chemical and Metallurgical Engineering, University of the Witwatersrand, Jorissen St, Johannesburg 2000, South Africa
[c] Institute for Nanotechnology and Water Sustainability (iNanoWS), College of Science, Engineering, and Technology, University of South Africa, Florida Science Campus, Johannesburg, 1710, South Africa

ARTICLE INFO

Keywords:
Dyes
Photocatalyst
Biochar
Photodegradation
UV-irradiation

ABSTRACT

The untreated release of dye-contaminated effluents into water bodies presents serious threats to both environmental and public health. Efficient dye removal methods are critical for preventing pollution and safeguarding ecosystems. This study aims to optimize the photocatalytic degradation of Eriochrome Black T dye in aqueous solutions using a novel composite of TiO_2 and biochar (BC) as a photocatalyst under UV irradiation. The TiO_2-BC composite (TBC-1) was synthesized via the sol-gel method and characterized using X-ray diffraction, BET surface area analysis, Fourier-transform infrared spectroscopy, Raman spectroscopy, and scanning electron microscopy with energy-dispersive X-ray spectroscopy. The synthesis resulted in an anatase phase crystal structure, a reduced band gap of 2.69 eV, and a significant surface area increase from 38 m^2/g to 78 m^2/g. The photocatalytic performance was optimized under UV light using Response Surface Methodology (RSM) with a Central Composite Design (CCD). Key variables, including initial pH (3–11), dye concentration (10–50 mg/L), photocatalyst dosage (0.5–2.5 g/L), and irradiation time (30–150 min), were assessed. An optimal decolorization efficiency of 99.14 % and a mineralization efficiency of 93.7 % were achieved at pH 3, 32 mg/L dye concentration, 1.48 g/L catalyst dosage, and 124 min irradiation time. These findings highlight the potential of the TBC-1 composite as an effective and sustainable solution for water and wastewater treatment applications, contributing to improved environmental management practices.

1. Introduction

Industrialization has driven significant economic growth and technological advancements, yet it has also led to considerable environmental damage. The burning of fossil fuels, the release of toxic chemicals, and the destruction of natural ecosystems have all contributed to widespread environmental pollution [1]. Among these issues, water pollution has become a global crisis, impacting billions of people by hindering economic progress and threatening both human health and environmental stability [2]. In addition to the scarcity of freshwater supplies, continuous degradation of water quality also contributes to global water scarcity. The primary factors contributing to this issue are urban development, industrial operations, and agricultural activities [3].

Industries, in particular, are major sources of water pollution, releasing hazardous substances that endanger the environment and public health. Among these, the textile sector is a major contributor, consuming large quantities of freshwater and discharging a substantial volume of contaminants, including, organic compounds, dyes, metals, and other harmful substances [4]. Dyes are essential for coloring products across various industries, including leather, cosmetics, textiles, and food. Synthetic dyes are extensively utilized in the textile industry, where azo dyes are most commonly used. These dyes account for two-thirds of the dyes used in textiles and over half of global dye production, with more than 2000 different types currently in use [5,6]. During the dyeing process, approximately 10–15 % of these dyes are

* Corresponding author.
E-mail addresses: nuramsh@gmail.com (M. Abdu), solomon.tibebu@aastu.edu.et (S. Tibebu), saeideh.babaee@wits.ac.za (S. Babaee), abebe.worku@aastu.edu.et (A. Worku), msagatam@unisa.ac.za (T.A.M. Msagati), fitojemal120@gmail.com (J.F. Nure).

https://doi.org/10.1016/j.rineng.2025.104036
Received 16 October 2024; Received in revised form 28 December 2024; Accepted 14 January 2025
Available online 14 January 2025

released directly into water bodies, contributing to significant environmental pollution. Dyes in water have the potential to create adverse health effects such as cancer, skin irritation, allergies, and dermatitis even in low quantities [7]. Azo dyes are particularly harmful due to their intense color and low degradation rate [8]. Eriochrome Black T (EBT), also referred to as Mordant Black 11, is an anionic azo dye, a commonly used anionic azo dye in the textile industry, is known for coloring a variety of fabrics, including silk, viscose, polyester, wool, nylon, and cotton [9,10]. This dye is environmentally hazardous, causing skin and eye irritation, and respiratory issues, and prolonged exposure can cause liver damage [10]. Despite its risks, EBT is widely used in developing countries, where effluents containing the dye are often released into water bodies without adequate treatment, posing a serious threat to the ecosystem [9,11]. Therefore, finding effective methods to remove EBT dye from wastewater is crucial to prevent further environmental damage and protect human health.

Various methods have been used to remove colors from wastewater, including biological treatment and chemical oxidation [12], adsorption, coagulation, flocculation, advanced oxidation processes (AOPs), and membrane filtration [13]. However, due to the properties of the dyes, common treatment methods are usually inefficient and may cause residual contamination [14]. Advanced oxidation processes, such as photocatalysis, Fenton, photo-Fenton, ozonation, and photolysis, have emerged as effective alternatives that can degrade persistent organic pollutants, including dye effluents, without generating secondary pollution [15]. These methods have the potential to be utilized either alone or in combination with other wastewater treatment techniques.

Heterogeneous photocatalysts are regarded as one of the most promising advanced oxidation processes (AOPs) for degrading persistent organic pollutants [16]. These catalysts are cost-effective, non-toxic, and exhibit strong biological and chemical stability [17]. Commonly used semiconductors in this process include ZnO, TiO_2, WO_3, CeO_2, SnO_2, ZrO_2, ZnS, and CdS [16]. TiO_2 is widely used as a photocatalyst due to its good catalytic performance, cost-effectiveness, abundance, high chemical stability, non-toxic nature, biological inertness, and reusability [18]. However, its large energy band gap (3.0–3.2 eV) restricts its application to the UV light spectrum, which makes up only about 7 % of sunlight [7,19]. Additionally, the difficulty of recycling nano-TiO_2 catalysts limits their broader applications. To improve TiO_2's photocatalytic efficiency and ease of recycling, various modifications have been made, including doping with metals such as Mn, Pt, Fe, Se, Cr, Ag, and Cu [20], non-metal elements like C, N, B, and P [21], combining with other semiconductor materials like ZnO, WO_3, SnO_2, and CdS [19], and integrating with adsorbent materials [22].

Combining TiO_2 with carbon-based materials has garnered attention due to its strong adsorption properties and its ability to enhance photocatalysis [22,23]. The strong interaction between TiO_2 and carbonaceous materials promotes their synergistic effects, increasing adsorption capacity and improving photocatalysis by enhancing the contact between pollutants and photocatalysts [24,25]. This approach also allows for easy separation of photocatalysts from effluents and enables their continuous reuse [22]. While activated carbon is often used as a support for TiO_2, the presence of numerous microporous structures can impede the diffusion of organic pollutants to the catalyst surface, and TiO_2 may obstruct these pore structures [26]. In contrast, biochar, with its larger pore structures and higher electrical conductivity, offers better support for TiO_2 and can enhance its photocatalytic performance in dye oxidation [26].

Biochar is a carbonized material derived from biomass waste, characterized by high stability and a strong capacity for pollutant adsorption [27,28]. The material's high stability and semiconductor properties make it a good support for TiO_2 [29]. The synergistic effects of TiO_2 and biochar composites significantly enhance TiO_2's photocatalytic efficiency, as biochar functions as an electron acceptor, aiding in the transfer of electrons from the TiO_2 surface and enhancing the separation of electron-hole pairs [26]. Biochar-photocatalyst composites have gained attention in various environmental applications. Some examples include TiO_2-reed straw [30], TiO_2-Salvinia Molesta [31], TiO_2-bamboo [32], TiO_2-coconut shell [33], TiO_2-corn cob [34], and TiO_2-ramie char [35].

Despite the known advantages of giant reed-derived biochar, research specifically targeting its integration with photocatalytic oxidation of EBT dye remains limited. Although the giant reed is known as one of the most dangerous invasive species worldwide, its biomass offers a low-cost alternative for biochar production, which is often underutilized in this context [36]. Existing studies have demonstrated the remarkable characteristics of giant reed-derived biochar, with a surface area of 506.3 m^2/g and a pore volume of 0.45 cm^3/g, demonstrating its potential to improve water purification through adsorption processes [37]. However, the influence of various factors such as pH, reaction time, catalyst dosage, and pollutant concentration on photocatalytic efficiency has not been thoroughly explored in conjunction with this specific composite [38]. In recent years, various optimization techniques have been utilized in process engineering to improve efficiency and accuracy. Among these, Response Surface Methodology (RSM) stands out for its advantages, particularly in optimizing complex experimental processes. One of its primary benefits is the capability to minimize the number of experiments needed by analyzing the effects of multiple variables simultaneously, saving both time and resources [39]. Unlike traditional methods that examine factors individually, RSM explores the interactions between variables, providing a more comprehensive understanding of their collective impact. RSM employs full quadratic models that facilitate precise predictions based on a variety of parameter combinations, making it ideal for detailed optimization, as seen in photocatalytic degradation studies [40]. The contour and response surface plots generated by RSM allow for intuitive visualization of variable effects, helping to identify optimal conditions more effectively. Among the different RSM designs, Central Composite Design (CCD) and Box-Behnken Design (BBD) are the most commonly used. CCD is highly efficient in examining linear, interaction effects, and quadratic, and its flexible design makes it well-suited for larger factor spaces [41]. On the other hand, BBD is more cost-effective as it avoids extreme factor combinations, but it is less effective in detecting curvature compared to CCD [39]. For this study, CCD was chosen for its ability to precisely optimize variables and explore their interactions. Hence, this study aims to address this gap by developing a TiO_2-BC composite using giant reed biochar and optimizing the photocatalytic degradation of EBT azo dye from aqueous solutions under UV light using Response Surface Methodology (RSM) under Central Composite Design (CCD).

2. Materials and methods

2.1. Preparation of biochar and TiO_2-biochar composite

The Giant reed stem was air-dried, chopped into small pieces, then dried in an oven at 105 °C for 24 h. The dry biomass was ground and then passed through an 80–120 mesh screen. Then, the biochar was produced by slow pyrolysis using a muffle furnace at 600 °C for 2 h in a nitrogen environment [42]. TiO_2-biochar composites were prepared using the sol-gel method with Titanium (IV) tetrachloride ($TiCl_4$) (99.5 %). Initially, 10 mL of $TiCl_4$ was added to 150 mL of deionized water in a 1000 mL beaker placed in an ice bath and continuously stirred for 10 min. Subsequently, 100 mL of ethanol (96 %) was added to the $TiCl_4$ solution and stirred for 20 min. The entire process was conducted in a fume hood. Biochar was added based on the TiO_2 to biochar ratio wt%. (10:1,10:2 and 10:3) for separate $TiCl_4$ solutions. The mixture was vigorously stirred for 5 min, and then the solution was titrated with 4 M NH_4OH until the pH reached 7.5 [43]. The mixture was settled overnight, and then the supernatant was decanted. The gel was dried overnight at 110 °C in a drying oven. The dried composite was then ground with a mortar and calcined at 600 °C for 2 h in a muffle furnace, with a heating rate of 10 °C/min, under a nitrogen atmosphere at a flow rate of

10 L/min. The TiO_2-BC composite was then cooled to room temperature and labeled as TBC-1, TBC-2, and TBC-3. Furthermore, pure TiO_2 was prepared using the same procedure without adding biochar.

2.2. Characterization of TiO_2-biochar composite

The crystal phases of TiO_2 and TBC-1 were analyzed using X-ray diffraction (XRD) on a SHIMADZU XRD-6000. The crystalline size of the composite was then calculated using the Scherrer equation (Eq. 1). Surface morphology and elemental composition were analyzed using Scanning Electron Microscopy (SEM) (JSM-IT300 Joel, Tokyo, Japan) in combination with an EDX (Oxford X-MAXN). Surface functional groups were determined using an iS50 FTIR infrared spectrometer. Molecular interactions and chemical structures were investigated using a WITec Raman spectrometer. The BET-specific surface area was determined using a HORIBA (SA-9600) surface area analyzer. The band gap and UV–Vis diffuse reflectance spectra (DRS) were measured using a Shimadzu UV-3600PLUS spectrophotometer. The band gap of the composite was estimated using Tauc's plot, while the Kubelka-Munk equations (Eqs. 2 and 3) were utilized for direct band gap determination [44].

$$D = \frac{K\lambda}{\beta\cos(\theta)} \tag{1}$$

Where D is the average crystallite size (in nanometres), K is the shape factor (typically taken as 0.9), λ is the wavelength of the X-ray radiation (for Cu Kα, = 1.5406 A°, B is the FWHM of the peak in radians and θ represent Bragg angle in radians.

$$F(R_\infty) = \frac{(1 - R\infty)^2}{2R_\infty} \tag{2}$$

$$(\alpha hv)^2 = B(hv - E_g) \tag{3}$$

Where $R\infty$ is the reflectance of an infinitely thick specimen, α is the absorbance, h is the Plank constant, ν is ν is the frequency of the photon, B is a constant *and* Eg is the band gap energy [44].

2.3. Point of zero charge determination

The point of zero charge (pHpzc) for TiO_2, biochar, and the TBC-1 composite was determined using the salt addition method. About 0.2 g of each sample was added to a 20 mL solution of 0.01M NaCl, which was adjusted to a pH range of 3 to 11. The solution pH was modified using 0.1M HCl for acidification and 0.1M NaOH for basification to cover the entire pH spectrum. Each mixture was vigorously shaken for 24 h to ensure thorough interaction between the sample and the solution, after that the final pH of the solutions was measured [45].

2.4. Photocatalyst performance test

Photocatalytic experiments were performed using a 19 W ultraviolet lamp. This lamp emitted light at 254 nm and was positioned 25 cm above the reactor. In separate beakers, 0.1 g of each TiO_2 and TBC-1 Composite was added to 100 mL of a 20 mg/L EBT dye solution. The mixture underwent stirring in the dark for 30 min; this step allowed for adsorption equilibrium to be reached. Once this period was over, the UV light was turned on. The photodegradation process then took place over 2 h. At 30, 60, 90, and 120-min intervals, 5 mL aliquots were withdrawn from the beaker and centrifuged at 8000 rpm. The supernatant containing EBT dye was analyzed using UV–visible spectroscopy at 534 nm to determine dye degradation, while TOC analysis was performed using the QbD1200 TOC Analyzer. The decolorization efficiency and degradation were calculated using Eqs. (4) and (5).

$$Removal\ \% = \frac{C_0 - Ce}{C_0} * 100 \tag{4}$$

$$TOC\ (\%)Removal = \frac{\text{Initial TOC} - \text{Final TOC}}{\text{Final TOC}} TOC * 100 \tag{5}$$

Where C_0 is the initial dye concentration (mg/L), Ce is the equilibrium concentration (mg/L), and TOC refers to the total organic carbon before (Initial TOC) and after treatment (Final TOC), both measured in mg/L.

2.5. Design of experiments

The efficiency of photocatalysis was assessed through an experimental framework based on four operational parameters, as detailed in Table 1. This investigation was implemented using the Central Composite Design (CCD) approach and the Design-Expert software (Stat-Ease, Design-Expert 13). The Central Composite Design (CCD) is a factorial approach used to analyze at least four independent variables through randomized response surface methodology. In this study, four variables pH (3–11), dye concentration (10–50 mg/L), catalyst dosage (0.5–2.5 g), and reaction time (30–150 min) were systematically examined for their effects on photocatalytic color removal. Each factor was tested at five levels (-α, -1, 0, +1, +α). The experiments were conducted in duplicate, and the average results were reported. The required number of experiments is defined by Eq. 6.

$$N = K^2 + 2k + Cp \tag{6}$$

Where Cp represents the number of central points and k denotes the number of variables.

The CCD for four input parameters and five levels proposed 30 total experimental runs, including 16 factorial points,8 axial points, and 6 center points [46]. The factors and their levels as well as the response are presented in Table 2. The predicted response (Y) can be derived from the quadratic model equation (Eq. 7):

$$\gamma = \beta_0 + \sum_{i=1}^{k} \beta_i \chi_i + \sum_{i=1}^{k} \beta_{ii} \chi_i^2 + \sum_{i=1}^{k-1} \sum_{j>1}^{k} \beta_{ij} \chi_i \chi_j + \varepsilon \tag{7}$$

Here, γ indicates the response to be optimized; b_0 is the constant coefficient; bi is the linear coefficient; bii is the quadratic coefficient; bij is the interaction coefficient; k represents the number of independent variables, ε denotes the unknown error constant, and xi and xj indicate the coded values of the independent factors.

The significance of the model, along with the assessment of individual and interaction effects of the factors, was analyzed using analysis of variance (ANOVA). The model's effectiveness was determined by evaluating the R^2, adjusted R^2 coefficient, and lack-of-fit tests. Optimal conditions were predicted by analyzing p-values and F-values, and 3D surface graphs were created to demonstrate the results.

2.6. Determination of reactive oxygen species

Scavenging experiments were conducted to identify the reactive species responsible for the EBT dye photodegradation process. The experiments compared the degradation rates of dye solutions with and

Table 1
Experimental design matrix for input variables and levels.

Factors	-alpha	Low (−1)	Mid (0)	High (+1)	+ alpha
pH	3	5	7	9	11
Catalyst load (mg/L)	0.5	1	1.5	2	2.5
Dye concentration (mg/L)	10	20	30	40	50
Time (min)	30	60	90	120	150

Table 2
Central composite design matrix.

Std	Run	Factor 1 A: pH	Factor 2 B: Catalyst Dose (g/L)	Factor 3 C: Dye Concentration (mg/L)	Factor 4 D: Time (min)	Response 1 EBT Removal (%)
1	18	5	1	20	60	83.84
2	15	9	1	20	60	55.53
3	30	5	2	20	60	93.09
4	3	9	2	20	60	71.52
5	1	5	1	40	60	73.65
6	25	9	1	40	60	50.89
7	2	5	2	40	60	82.87
8	16	9	2	40	60	67.85
9	17	5	1	20	120	95.73
10	26	9	1	20	120	71.51
11	27	5	2	20	120	99.12
12	13	9	2	20	120	82.82
13	8	5	1	40	120	86.33
14	28	9	1	40	120	66.55
15	9	5	2	40	120	90.59
16	21	9	2	40	120	78.52
17	5	3	1.5	30	90	98.9
18	19	11	1.5	30	90	56.89
19	11	7	0.5	30	90	61.94
20	29	7	2.5	30	90	81.05
21	6	7	1.5	10	90	91.86
22	20	7	1.5	50	90	75.9
23	24	7	1.5	30	30	68.3
24	12	7	1.5	30	150	89.23
25	7	7	1.5	30	90	84.76
26	22	7	1.5	30	90	85.43
27	23	7	1.5	30	90	85.56
28	10	7	1.5	30	90	84.82
29	4	7	1.5	30	90	85.78
30	14	7	1.5	30	90	85.65

without the addition of scavengers. Specifically, n-butanol (n-but) was introduced at a concentration of 0.05 mol to scavenge hydroxyl radicals (·OH), ascorbic acid (AA) at 0.001 mol to target superoxide radicals ($\cdot O_2$), and oxalic acid (OA) at 0.05 mol to scavenge holes (h^+) [47].

2.7. Photodegradation kinetics study

The kinetics of EBT photocatalytic degradation were investigated under optimum experimental conditions. The degradation process was modeled using first-order kinetics (Eq. 8). Before starting the photodegradation procedure the solution was stirred in the dark for 30 min to reach adsorption equilibrium [48]. The UV light was activated, and the photodegradation was conducted over 2 h. Samples of 5 mL were taken at intervals of 20, 40, 60, 80, 100, and 120 min. These samples were centrifuged at 8000 rpm, and the supernatant with the remaining EBT dye was examined using UV-visible spectroscopy with an absorption wavelength of 534 nm.

$$\ln\left(\frac{Ct}{Co}\right) = -kt \tag{8}$$

Where Ct denotes the concentration at time t, Co is the initial dye concentration, and k is the first-order rate constant.

2.8. Recycling test

The recycling test was conducted using optimized parameters. About 0.15 g of the catalyst was added to a 500 mL beaker containing 100 mL of a 32 mg/L Erichrome Black T dye solution. After each experiment, the mixture was allowed to settle for 30 to 60 min, then the supernatant solution was carefully removed with a micropipette from the beaker without disturbing the catalyst. Subsequently, the experiment was restarted by adding 100 mL of a 32 mg/L dye solution to the reaction beaker. The process was repeated five times.

3. Result and discussion

3.1. Characteristics of TiO_2-BC composite

3.1.1. XRD analysis

The X-ray diffraction (XRD) patterns of BC, TiO_2, and the TBC-1 composite are presented in Fig. 1. The XRD spectrum for BC shows two wide peaks at 23.5° (C (002)) and 43.5° (C (100)), signifying the orientation of aromatic carbon structures and diffraction of graphitic and hexagonal carbons [49]. In contrast, the XRD patterns for TiO_2 and the TBC-1 composite show diffraction peaks at 25.3°, 38.1°, 48.2°, 54.1°, 54.9°, 62.8°, and 69.3°, which correspond to the (101), (004), (200), (105), (211), (204), and (220) planes, respectively, indicating the anatase crystal form of TiO_2 (PDF-2 00–064–0863). This indicates that the incorporation of biochar does not substantially change the crystallographic structure of TiO_2. However, the peaks of the TBC-1 composite are slightly wider than pure TiO_2, as observed in Fig. 1. This finding aligns with previous studies [47,50]. The absence of BC peaks in the composite suggests that the anatase TiO_2 may have altered or masked the graphitic carbon structure of the biochar, possibly due to the strong anatase TiO_2 peaks overshadowing the weaker BC peaks [47]. On the other hand, the incorporation of biochar into TiO_2 catalysts reduces the crystallite size from 40.6 nm to 22.8 nm, enhancing the material's photocatalytic properties. This reduction is attributed to several mechanisms: biochar provides additional nucleation sites, promoting smaller TiO_2 crystallites, while its porous structure inhibits particle agglomeration during synthesis [51]. Biochar also influences thermal properties, stabilizing smaller TiO_2 particles at elevated temperatures, and its functional groups may interact with TiO_2 precursors, modifying the crystallization process [52]. The large surface area and porous structure promote the even distribution of TiO_2 nanoparticles, resulting in more uniform growth [53,54]. Smaller TiO_2 particles have a larger surface area-to-volume ratio, increasing active sites for reactions and improving photocatalytic efficiency in processes of wastewater treatment and air purification [55]. The reduced size also facilitates better light absorption, charge separation, and quantum size effects, which lower the band gap energy for enhanced visible light absorption [56]. Additionally, smaller crystallites improve TiO_2 dispersion in matrices, enhancing composite performance [57]. These characteristics make reduced crystallite size crucial for optimizing TiO_2 in various sustainable applications. Additionally, the recycled TiO_2-BC (R-TBC-1) composite exhibits a spectrum similar to that of the original TBC-1 composite, with the primary differences observed in the peak intensity and a reduction in crystalline size from 22.8 nm to 20.3 nm. This reduction in crystalline size may enhance degradation performance by increasing the available

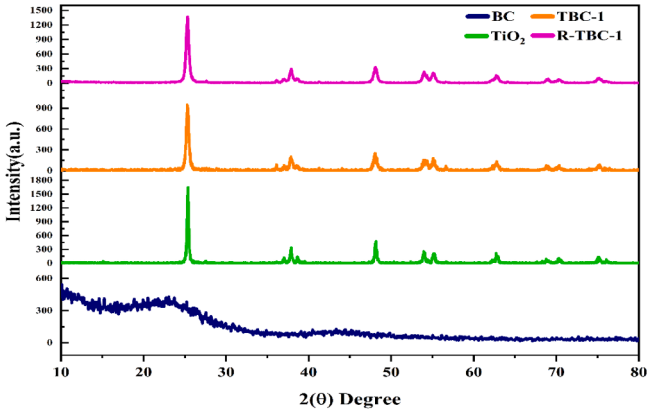

Fig. 1. X-ray diffraction (XRD) pattern of BC, TiO_2, TBC-1, and R-TBC-1 composite.

surface area and improving photocatalytic activity. The increased intensity of the XRD peaks for the recycled catalyst could be attributed to interactions and mechanical effects caused by the magnetic stirrer and the reactor during the recycling process. Furthermore, the reduction of biochar in the composite might contribute to the observed increase in crystallinity, which is a favorable property for the catalyst's reuse across multiple cycles.

3.1.2. Raman spectroscopy

Raman spectroscopy was used to analyze the TiO_2-biochar composite, focusing on both the TiO_2 and its biochar composite form as well as the carbon matrix. The Raman spectra for TiO_2, BC, and TBC-1, shown in Fig. 2, reveal distinct peaks at 143 cm^{-1} (Eg), 196 cm^{-1} (Eg), 394 cm^{-1} (B1g), 514 cm^{-1} (A1g), and 634 cm^{-1} (Eg). These peaks represent the anatase phase of TiO_2 [58]. There were no rutile or other TiO_2 phase peaks found in the TiO_2-biochar composite. Additionally, the Raman spectra of the TBC-1 composite show two extra peaks at 1350 cm^{-1} (D) and 1595 cm^{-1} (G), corresponding to the presence of sp^3 C–C atoms and sp^2 C–C bonded carbon molecules of biochar [59]. The D peak, a defect-derived peak, indicates disorder, while the G peak represents graphitic carbon. The inclusion of biochar in the TBC-1 composite is evident from these distinct biochar peaks. The presence of biochar also reduces the intensity of the TiO_2 peaks, suggesting that the TiO_2 nanoparticles have successfully integrated with the biochar material to form the TBC-1 composite. This integration is crucial for enhancing the catalytic properties of the TiO_2 nanoparticles, as the biochar provides a stable support structure for the nanoparticles to adhere to.

3.1.3. FTIR spectrum analysis

Fig. 3 shows the FTIR spectra of BC, TiO_2, and TiO_2-biochar composite. In the TBC-1 and the recycled TBC-1 composite, a broad peak at 3395 cm^{-1} is associated with the stretching vibrations of O-H bonds from phenolic, hydroxyl, and carboxyl groups, along with water adsorbed on the surface of the catalyst [26]. Notably, this peak is absent in both the Biochar and TiO_2 spectra, suggesting a chemical interaction between the biochar and TiO_2 materials. Additionally, the TBC-1 and (R-TBC-1) composite show a medium-wide peak at 1640 cm^{-1}, indicating the presence of C=O and C=C bonds in biochar carboxylate and aromatic molecules [60]. This may be due to interactions during the reaction involving NH_4OH, ethanol, and TiO_2 which could lead to the incorporation of hydroxyl (OH) and other functional groups. The spectra of the TiO_2 composite show an absorption band in the 600–400 cm^{-1} region, which is attributed to the stretching vibrations of the Ti-O and Ti-O-Ti bonds in TiO_2; however, no corresponding features are present in the BC spectrum [61]. The modification of TiO_2 in the composite is evident,

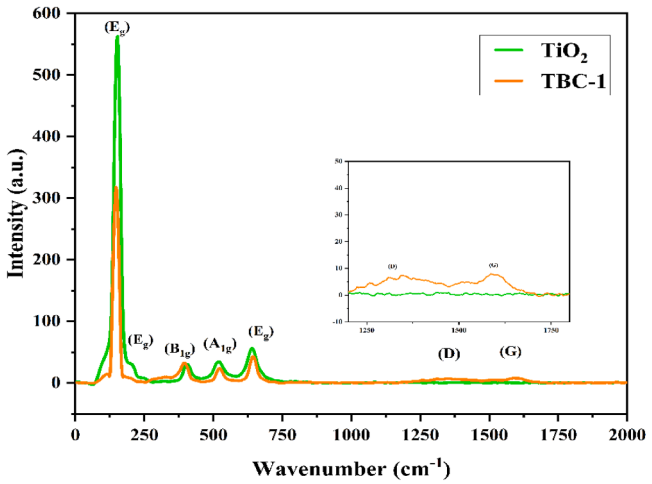

Fig. 2. Raman spectrum for TiO_2 and TBC-1 composite.

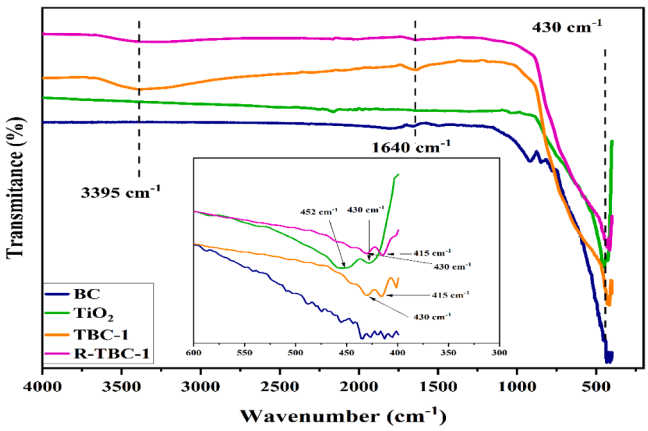

Fig. 3. FTIR spectra of BC, TiO_2,TBC-1, and R-TBC-1.

as the absorption band shifts from 450 and 430 cm^{-1} in pure TiO_2 to 430 and 415cm^{-1} in the TBC-1 composite. The addition of biochar shifts and narrows the TiO_2 absorption bands, indicating a modification of the TiO_2 bond structure. This shift indicates the formation of C-Ti-O bonds and a reduction in the Ti-O-Ti bond length within the TiO_2 molecule, likely resulting from the doping process. FTIR analysis revealed that the functional groups of the recycled TBC-1 (R-TBC-1) catalyst remained unchanged even after five consecutive cycles. This finding demonstrates the high stability of the TBC-1 catalyst and its ability to maintain consistent performance throughout the recycling process.

3.1.4. SEM-EDX analysis

Scanning Electron Microscopy (SEM) and Energy-Dispersive X-ray (EDX) analyses were performed to investigate the microstructure, morphology, and elemental composition of the composite material. Fig. 4(a and b) presents SEM images of both pure TiO_2 and the TiO_2-biochar composites. The SEM analysis provides crucial insights into the structural and morphological characteristics of the TiO_2-biochar composite. The SEM image of pure TiO_2 reveals smooth and uniform particles, while the TiO_2-biochar composite exhibits a rough and cracked surface. The incorporation of biochar significantly impacts the TiO_2 surface texture, as evidenced by the rough and cracked surface of the composite in contrast to the smooth surface of pure TiO_2, indicating enhanced surface area and porosity. These features are important for catalytic applications as they enhance the adsorption capacity and improve interactions between the catalyst and pollutants [62]. This enhancement can accelerate the degradation process and simplify the separation of photocatalysts from the effluent, enabling repeated use [22]. The images of the recycled TBC-1 (R-TBC-1) catalyst after five cycles of photodegradation show a similar structure to the original, indicating that the catalyst surface retains its integrity even after repeated use. However, Fig. 4c presents the R-TBC-1 images, showing some agglomerated and larger TiO_2 particles on the biochar surface, indicating minor structural alterations during the recycling process. The EDX analysis was conducted to identify the components of the composite and their distribution. Fig. 5 illustrates the elemental composition of both TiO_2 and the TiO_2-biochar composite. The EDX analysis in Fig. 5a shows that the pure TiO_2 sample consists of 57.8 wt% titanium and 43.2 wt% oxygen. In contrast, the TiO_2-biochar composite (Fig. 5b) contains 47.2 wt% titanium, 39.6 wt% oxygen, and 13.2 wt% carbon. The presence of carbon in the composite, absent in pure TiO_2, indicates that biochar particles are effectively integrated into the TiO_2 matrix. This integration alters the surface properties and enhances the overall functionality of the composite. The reduction in titanium and oxygen weight percentages in the composite compared to pure TiO_2 reflects the addition of biochar, which contains a significant amount of carbon. The higher carbon content in the composite is attributed to biochar

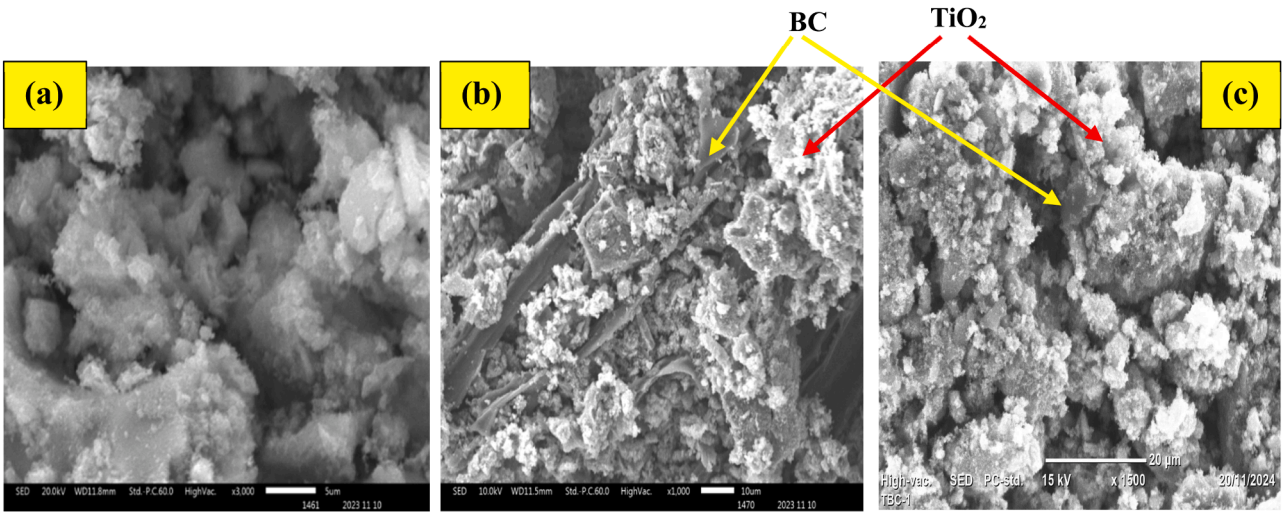

Fig. 4. SEM image (a), TiO_2, (b), TBC-1 composite and (c), R-TBC-1.

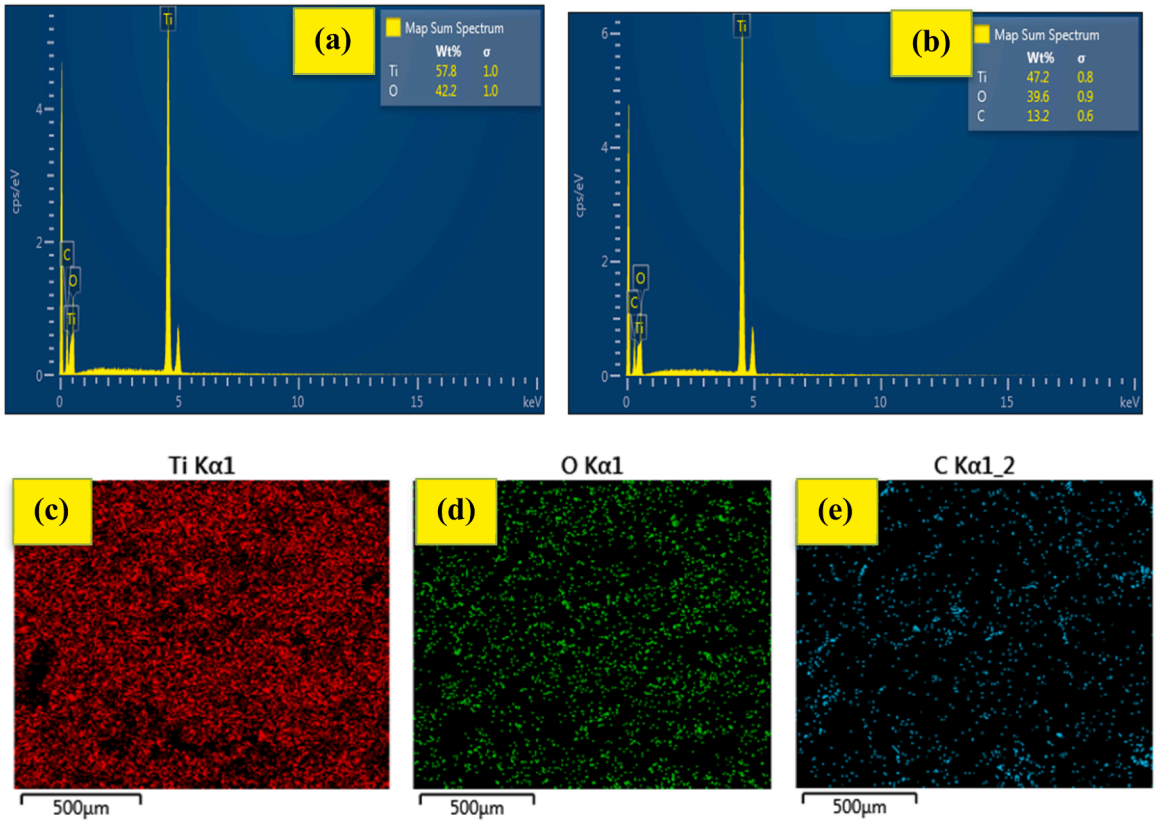

Fig. 5. The EDS analysis result for (a) TiO_2, (b) for TBC-1 composite, and (c-e) for TBC-1 composite elemental mapping.

microparticles covering the TiO_2 nanoparticles. The EDX analysis provides an examination of the surface microdomain, influenced by the sample surface depth, typically up to one micron below the surface [26].

3.1.5. Surface area analysis

A surface area analyzer was used to determine the surface area of TiO_2, biochar, and the TiO_2-biochar composite. The results indicate that the BET surface areas were 428.98 m^2/g for biochar, 38 m^2/g for bare TiO_2, and 78 m^2/g for the TBC-1 composite. The surface area analysis shows the importance of biochar in improving the characteristics of TiO_2 catalysts. The addition of 10 % biochar to TiO_2 nearly doubled its surface area, greatly improving the adsorption capacity and effectiveness of the photocatalytic reactions. This is due to the unique pore structure of biochar, which provides additional surface area and serves as a support for TiO_2 nanoparticles. Additionally, the incorporation of biochar into TiO_2 significantly contributes to reducing the crystallite size of TiO_2 as described in Section 3.1. Biochar acts as an additional nucleation site, promoting the formation of smaller TiO_2 crystallites, while its porous structure effectively inhibits particle agglomeration during synthesis [51]. Furthermore, the high surface area and porosity of biochar enhance the dispersion of TiO_2 nanoparticles, facilitating more uniform growth [54]. The resulting smaller TiO_2 particles exhibit a

higher surface area-to-volume ratio, which increases the availability of active sites for chemical reactions. This enhancement directly improves photocatalytic efficiency in applications such as wastewater treatment and air purification, making the TiO_2- biochar composite a highly effective material for environmental remediation [55]. Catalysts with larger surface areas have a higher capacity to adsorb molecules because of the increasing number of active attachment sites [22]. Recent studies have shown that a TiO_2-biochar composite can achieve a surface area of 192 m^2/g [63], while an AC-TiO_2 composite reached 34.2 m^2/g [64]. Additionally, incorporating SiO_2 increased the specific surface area of an N-TiO_2 sample from 40.70 m^2/g to 115.4 m^2/g [65]. These findings highlight the importance of incorporating biochar and other materials to enhance the performance of TiO_2-based catalysts, as both components influence specific surface area. Prioritizing materials that maximize surface area is crucial for increasing active sites and achieving efficient photodegradation. Enhancing TiO_2 catalysts with biochar or other adsorbents significantly improves their effectiveness in environmental applications.

3.1.6. UV–vis DRS analysis of TiO_2-BC composite

Fig. 6 presents the UV–vis DRS spectra and band gaps of TiO_2 and the TBC-1 composite. The addition of biochar to TiO_2 results in induced ultraviolet absorption and visible light absorption. TBC-1 shows a redshifted maximum light absorption edge and enhanced absorption in the ultraviolet spectrum compared to pure TiO_2. The band gaps (Eg) of TiO_2 and TBC-1 were calculated using Tauc plots, yielding values of 3.03 eV and 2.69 eV, respectively. This redshift in absorption and reduction in band gap is related to the interaction between TiO_2 and biochar. When TiO_2 and biochar are combined, their electronic structures interact, creating new levels of energy within the TiO_2 band gap. These new levels, which are closer in energy, effectively reduce the overall band gap [66]. Additionally, biochar can act as a dopant, introducing impurities that further narrow the band gap [67]. Another study reported a decrease in the band gap of anatase TiO_2 from 3.40 eV to 2.44 eV with the addition of biochar [44]. These findings indicate that the TiO_2-biochar composite has a broader absorption range compared to pure TiO_2, suggesting an enhancement in photocatalytic efficiency. Consequently, the TiO_2-biochar composite can absorb light across a wider range of wavelengths, improving its photocatalytic performance.

3.1.7. Point of zero charge (pHpzc)

Determining the point of zero charge (pHpzc) is essential for understanding the surface chemistry of catalyst materials and developing effective water remediation techniques. The pHpzc helps to control the degradation process by analyzing the catalyst surface charge relative to the water pH. Adsorbents above the pHpzc attract positively charged contaminants, while those below it typically attract negatively charged contaminants [68]. The pHpzc of TiO_2 is around 5.56, as shown in Fig. 7, indicating that TiO_2 has a positively charged surface below and a negatively charged surface above this pH. This value aligns with previous research and may impact its practical applications [69]. In contrast, biochar has a pHpzc of 8.6, and when combined with TiO_2, the pHpzc shifts to 6.28 for the TBC-1. This shift from acidic to neutral pHpzc is influenced by the biochar's characteristics and quantity. The increased pHpzc of the composite expands its effectiveness across a broader pH range, making it suitable for removing anionic pollutants. This enhanced versatility improves the catalyst's efficiency in contaminant removal from water and other environmental systems.

3.2. Photodegradation experiment

The photocatalytic oxidation of EBT dye was evaluated compared to TiO_2 and TiO_2-biochar composite catalysts under UV irradiation. Fig. 8 demonstrates that the degradation of EBT dye utilizing pure TiO_2 catalysts achieved only 78.04 %, indicating a substantial challenge in degrading the entirety of the dye molecule compounds and their intermediates. Conversely, applying TiO_2-biochar composite catalysts led to a notable enhancement in degradation efficiency, attaining a dye degradation rate of 87.58 %, 83.15 %, and 71.41 % for TBC-1, TBC-2, and TBC-3 respectively. These results suggest that the TiO_2-biochar

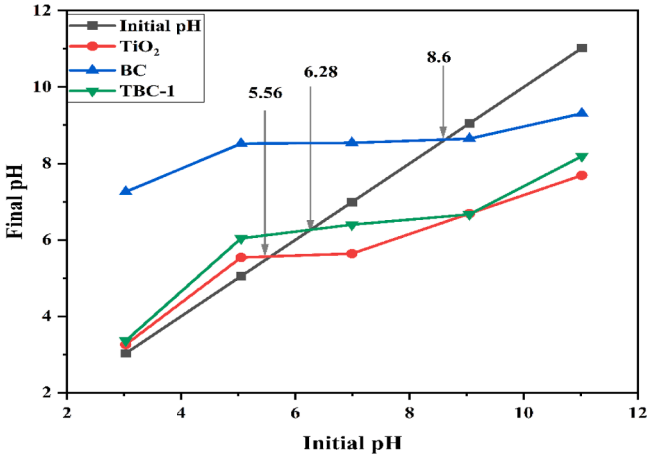

Fig. 7. Point of zero charges (pHpzc) of Biochar, TiO_2 and TBC-1 composite.

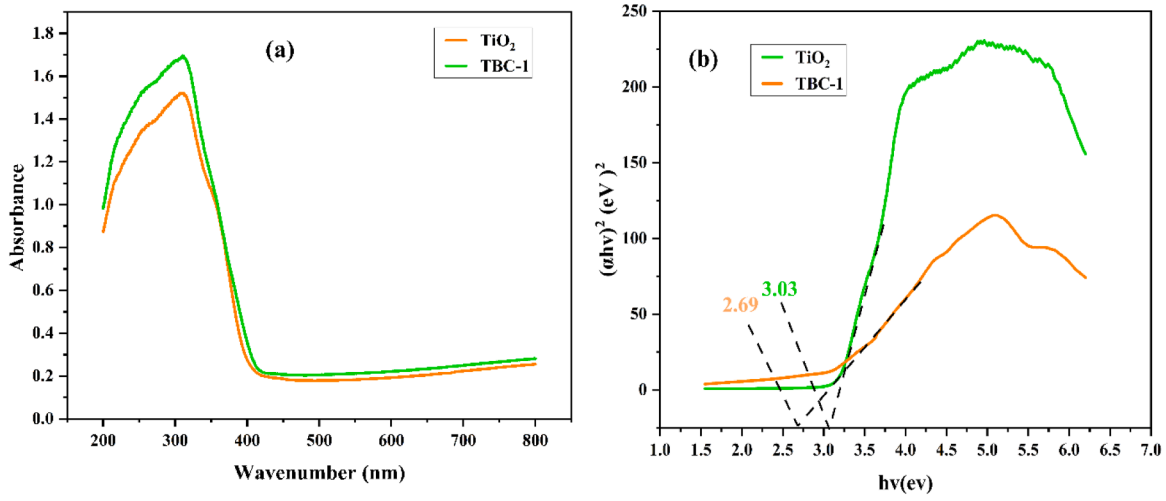

Fig. 6. UV–vis diffuse reflectance spectra(a) and energy band gap(b) for TiO_2 and TBC-1 composite.

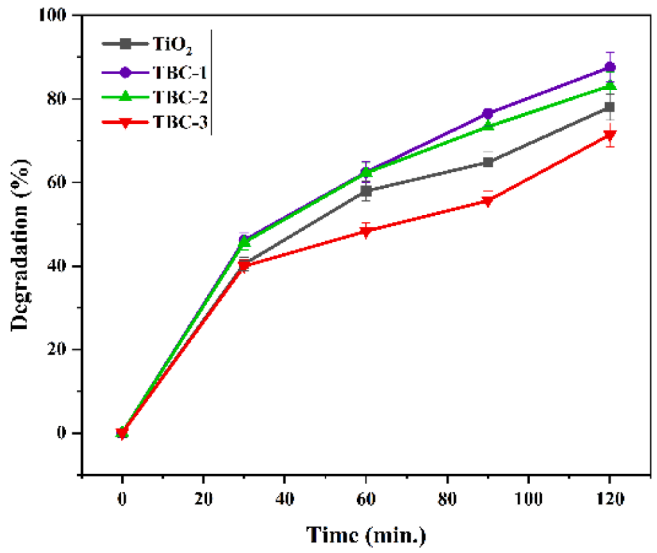

Fig. 8. Comparative efficiency of TiO_2, TBC-1, TBC-2, and TBC-3 composite on the degradation rate of EBT dye, Conditions: Catalysts dose, 0.1 g; [dye], 20 mg/L; solution, 100 mL; UV irradiation time, 120 min.

composite exhibited superior performance relative to the pure TiO_2 catalysts except TBC-3. The incorporation of biochar facilitated the targeted pollutants' adsorption onto the catalyst surface and provided the possibility of transforming photoelectrons, which reduced the electron-hole pairs recombination, resulting in the interaction between TiO_2 and biochar [22,26]. The interaction significantly impacted the effectiveness of the photocatalytic oxidation process. Additionally, the inclusion of biochar contributed to a reduction in the energy band gap of the pure TiO_2 catalyst, which in turn promoted the generation of active species and expedited photo-oxidation reactions [44]. However, the degradation performance of biochar-doped TiO_2 photocatalysts declines when the biochar content exceeds 20 wt.%. This reduction occurs because increased biochar can saturate the effective surface area, thereby limiting active sites for pollutant adsorption [52]. Furthermore, excessive biochar can obstruct light penetration, which hinders photocatalytic activity [70]. An imbalance in the TiO_2 to biochar ratio can also disrupt electron transfer, leading to diminished photocatalytic efficiency [71]. Therefore, optimizing biochar loading is essential for enhancing photocatalytic performance. Ultimately, the TiO_2-biochar composite emerges as a potent photocatalyst for the oxidation of azo dyes, the TBC-1 demonstrating a significantly higher degradation rate of EBT compared to pure anatase TiO_2.

3.3. Model fitting and analysis of variance (ANOVA)

3.3.1. Model fitting analysis

The catalyst dose, reaction time, pH, and dye concentration were optimized through Response Surface Methodology (RSM) and Central Composite Design (CCD) to improve the degradation efficiency of EBT dye, as outlined in Table 2. An analysis of variance (ANOVA) was conducted to determine the model's statistical significance. According to Table 3, the quadratic regression model is the most suitable for analyzing EBT dye photodegradation, as indicated by the F-value, P-values, and R^2. The results indicate that the quadratic model's regression has an F-value of 4685.53 and a very low p-value (<0.0001), suggesting that the model is highly significant. The adjusted R^2 and coefficient of determination (R^2) were used to assess the model's performance. The results indicate an excellent fit, with an R^2 of 0.9985 and an adjusted R^2 of 0.9972, demonstrating that the selected model can present 99.72 % of the response data. Furthermore, the predicted R^2 of 0.9925 nearly aligns with the adjusted R^2, indicating a strong connection between the experimental and predicted models. The low coefficient of variation (C. V. %) of 0.84 % indicates that the experimental data is precise, reliable, and reproducible. Additionally, The Adequate Precision value of 102.5, well above the acceptable threshold of 4, shows that the model is highly reliable for predicting EBT dye degradation using the TBC-1 composite catalyst [72]. The ANOVA table for the quadratic model offers important information about the significance of the model terms and how they influence the degradation efficiency of the process [72]. As illustrated in Table 3 The large F-value and the small p-value (<0.05) provide additional evidence in explaining the variation in degradation efficiency. The P-values for each model term provide additional insights, with terms having p-values less than 0.05 being considered statistically significant. In this study, factors A (pH), B (catalyst dosage), C (dye concentration), and D (degradation time), as well as the interactions AB, AC, AD, BD, and the quadratic terms A^2, B^2, C^2, and D^2, are all identified as significant contributors to the model. The low p-values for these factors demonstrate their strong influence on degradation efficiency. On the other hand, the interactions BC and CD have p-values greater than 0.05 (0.37 and 0.57), indicating that they are not statistically significant in this model. Additionally, the Lack of Fit F-value of 3.07 indicates that the Lack of Fit is not statistically significant when compared to the pure error, with noise accounting for an 11.35 % probability of explaining such a high Lack of Fit F-value. A non-significant Lack of Fit in ANOVA

Table 3
Analysis of variance (ANOVA) results for Photodegradation quadratic model.

Source	Sum of Squares	df	Mean Square	F-value	p-value	Significant
Model	4685.53	14	334.68	737.29	< 0.0001	#
A-Ph	2481.68	1	2481.68	5467.06	< 0.0001	#
B-Catalyst dose	605.71	1	605.71	1334.37	< 0.0001	#
C-Dye concentration	321.42	1	321.42	708.08	< 0.0001	#
D-Time	745.82	1	745.82	1643.02	< 0.0001	#
AB	56.66	1	56.66	124.83	< 0.0001	#
AC	26.96	1	26.96	59.40	< 0.0001	#
AD	14.61	1	14.61	32.19	< 0.0001	#
BC	0.3813	1	0.3813	0.8400	0.3739	##
BD	26.24	1	26.24	57.81	< 0.0001	#
CD	0.1463	1	0.1463	0.3223	0.5786	##
A^2	92.45	1	92.45	203.67	< 0.0001	#
B^2	323.81	1	323.81	713.35	< 0.0001	#
C^2	3.16	1	3.16	6.97	0.0185	#
D^2	71.84	1	71.84	158.27	< 0.0001	#
Residual	6.81	15	0.4539			
Lack of Fit	5.86	10	0.5856	3.07	0.1135	##
Pure Error	0.9527	5	0.1905			
Cor Total	4692.34	29				

R^2 = 0.9985, Adj. R^2 = 0.9972, Pre. R^2=0.9925, C.V.%=0.847, Adeq Precision = 102.54, Significant = #, and Not-significant = ##

for regression models indicates that the model adequately fits the data, as any discrepancy between observed and predicted values is likely due to random variation rather than model inadequacy [73]. This result indicates that the model accurately represents the relationship between variables without requiring additional complexity. With a p-value above the chosen significance level (0.05), the Lack of Fit test supports the model's sufficiency in describing the data, confirming that residuals are randomly distributed and that the model's predictions align well with observed values [39]. Hence, a quadratic polynomial equation (Eq. 9) was utilized to estimate the effectiveness of photocatalysts on EBT dye oxidation considering the independent variables.

$$\text{Color Removal } (\%) = 84.94 - 10.16{*}A + 5.02{*}B - 3.65{*}C + 5.57{*}D + 1.88{*}AB + 1.29{*}AC + 0.95{*}AD - 1.28{*}BD - 1.78 * A^2 - 3.38 * B^2 - 1.56 * D^2 \quad (9)$$

Where A represents the solution pH, B is the catalyst dose, C denotes the initial dye concentration, and D stands for the reaction time.

The impact of a variable is defined by the change in the outcome resulting from adjusting that variable's level. The formula presented in Eq. (9) is a quadratic equation (coded according to the factors) for the analyzed response, with an intercept coefficient set at 84.94. Increasing the catalyst dose (B) and reaction time (D) enhances decolorization efficiency, as indicated by their positive coefficients of 5.02 and 5.57, respectively. This improvement is likely because a higher catalyst dose creates more active sites for the reaction, and a longer reaction time allows for more complete interaction between the dye and the catalyst. Conversely, pH (A) and initial dye concentration (C) negatively impact the degradation performance, with coefficients of -10.16 and -3.65, respectively. Higher pH might affect the stability of the catalyst or the ionization state of the dye, reducing reaction efficiency. Similarly, a higher initial dye concentration could lead to saturation effects where the catalyst's active sites are insufficient to handle the excess dye. Interaction effects (AB), (AC), and (AD) also show positive influences, with values of 1.88, 1.29, and 0.95 respectively. Conversely, interaction effects of (BD), (A^2), (B^2), and (D^2) display negative coefficients of -1.28, -1.83, -3.43, and -1.61 respectively. The positive interaction effects suggest synergistic relationships where the combined influence of two variables is greater than the sum of their individual effects. In contrast, negative interaction effects imply that certain combinations or high levels of individual variables can detrimentally impact the process. The significance of all factors, including both individual and interaction factors (except BC and CD), is determined by their p-values. Table 3 shows that the linear components A, B, C, and D, as well as their interactions with other factors, have p-values less than 0.05, suggesting that they are important in the degradation of EBT dye. These p-values guide which factors are critical to consider in the decolorization process. Furthermore, the sum of squares (SS) from the ANOVA data was utilized to calculate the total percentage contributions (TPC) of each variable using Eq. 10, representing the proportion of variance explained by each factor. As illustrated in Fig. 9, the individual effects dominate over the interactive and quadratic effects, aligning with findings in the literature [73]. Among the individual factors, pH emerges as the most influential, followed by degradation time and catalyst dose, with the quadratic effect of the catalyst dose also playing a significant role. Dye concentration exhibits the least impact among the individual factors, while all interaction and remaining quadratic effects contribute less than 5 %. By focusing on the significant variables and their optimal levels, it is possible to enhance the efficiency of EBT dye degradation effectively.

$$Contribution = \left(\frac{\text{Sum of Squares}}{\text{Total Sum of Squares}}\right) * 100 \quad (10)$$

3.3.2. Validation of the RSM model

A validation assessment is crucial for developing an accurate mathematical model. The model's validity was confirmed by comparing the predicted responses to the actual experimental outcomes [74,75]. Fig. 10a shows a graph of the actual vs projected values, illustrating that all data points are scattered and normally distributed around the linear regression line. The normal distribution suggests that the errors are well-distributed. Fig. 10b presents the residual normality plot, demonstrating that the residuals follow a normal distribution. Fig. 10c, which plots residual values versus predicted values, demonstrates a random distribution without significant variance trends. Additionally, Fig. 10d presents the Internally Studentized Residuals diagram, showing no unusual points. These results indicate the suitability and accuracy of the CCD model for optimizing the EBT dye photodegradation process.

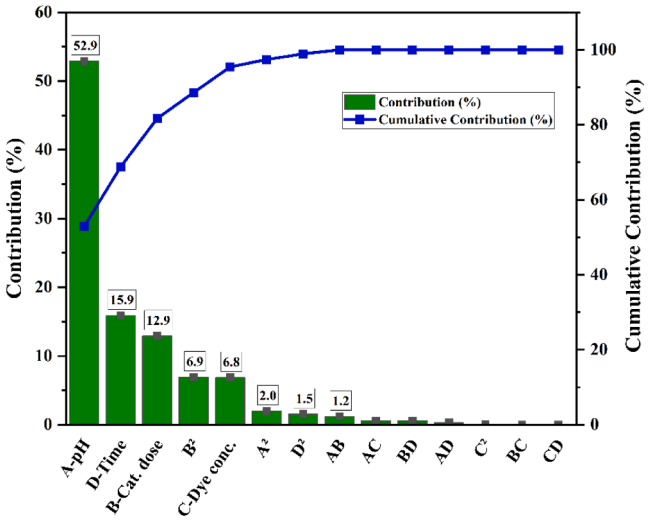

Fig. 9. Schematic representation of the Percentage Contribution.

3.4. Individual factor effects

The response surfaces are visually represented through quadratic regression equations and accompanying graphs. Fig. 11(a–d) illustrates the significant impacts of each factor on the response and the interactions between different factors. These graphs show the effects of individual factors pH (A), catalyst dose (B), initial concentration (C), and time (D) as well as their interactions on degradation efficiency. The pH of the reaction media is a critical factor in the photodegradation process, as it influences the surface charge and ionization of the catalyst [76]. The pH level can affect the photocatalytic degradation of pollutants by altering the catalyst surface properties, charge distribution on organic molecules, and the production of reactive radical species [77]. The effect of initial pH on the degradation process of EBT dye was studied in the range (of 3–11). The results, as illustrated in Fig. 10a, indicate that the degradation of Eriochrome Black T (EBT) is most effective under acidic conditions. Specifically, TBC-1 achieves an impressive degradation rate of 98.3 % at a pH of 3. However, as the pH level increases, the efficiency of degradation decreases, with rates of 93.6 %, 85.9 %, and 57.6 % observed at pH levels of 5, 7, and 11, respectively. Understanding the degradation behavior of the EBT dye relies heavily on the point of zero charge (pHpzc) of the TiO_2-BC (TBC-1) catalyst and the pKa values of the EBT dye. This dye is sensitive to pH and features two acidity constants, with pKa values of 6.2 and 11.5. Below a pH of 6.2, EBT mainly exists as monovalent anions in aqueous solutions [78]. The TBC-1 composite has a point of zero charge (pHpzc) of 6.28. This means that its surface carries a positive charge in acidic conditions (pH $<$ 6.28) and a negative charge when the pH is greater than 6.28. At lower pH levels, the negatively charged EBT molecules, which contain sulfonated (-SO_3-) groups, are attracted to the positively charged active sites on TBC-1 through electrostatic interactions [79].

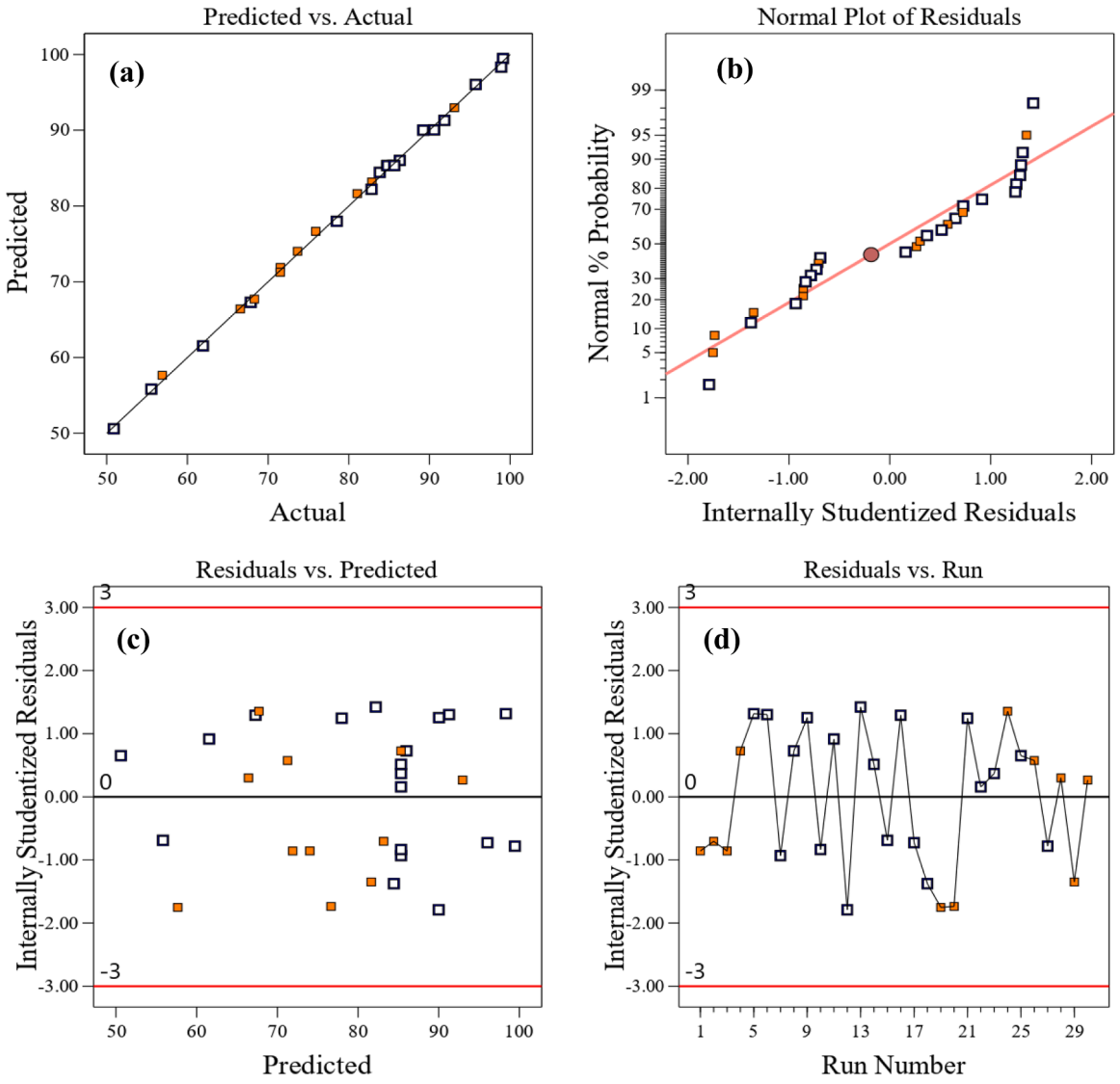

Fig. 10. (a) predicted vs actual values, (b) Normal plot of residuals, (c) Residuals vs predicted values, and (d) Residuals vs run.

This facilitates interactions with photogenerated holes and hydroxyl radicals (·OH), which target the aromatic rings, break azo bonds, and eliminate chromophoric groups, leading to effective degradation [78]. In contrast, at pH values above the pKa of EBT and the pHpzc of TBC-1, both the catalyst surface and the EBT dye acquire negative charges. The dye molecules transform into di or trivalent anionic sulfonated forms, leading to strong electrostatic repulsion between the catalyst and the dye [80]. Additionally, the presence of OH^- ions in the alkaline solution further suppresses the formation of ·OH radicals, significantly reducing photodegradation efficiency [78]. This combination of electrostatic repulsion and limited radical generation explains the decreased performance at higher pH levels. Similarly, the catalyst dosage is an important factor in the degradation process of EBT dye. As shown in Fig. 10b the degradation percentage increases from 61.5 % to 87.5 % when the catalyst dosage increases from 0.5 to 2 g/L. Increasing the photocatalyst dosage enhances the number of active sites and electron-hole pairs, resulting in a greater formation of active radicals. This enhances mass transfer and the photocatalytic degradation of EBT dye. Additionally, a higher dosage increases the available surface area, further improving EBT removal [75]. However, beyond 2 g/L, the degradation percentage experiences a slight decrease. Excess catalyst dosage can lead to particle agglomeration and reduced light penetration, ultimately decreasing the degradation rate [81]. A similar result reported the degradation of RV5 Azo Dye on Fe-Doped Titania Catalysts (0–6 g/L) under visible light irradiation showed a consistent degradation rate after reaching 3 g/L [82]. Hence, the optimal amount of catalyst must be added to ensure efficient photodegradation. The impact of the initial concentration of EBT on its degradation percentage was examined within a concentration range of 10 to 50 mg/L. As shown in Fig. 10c the maximum degradation percentage observed was 91.3 % at a concentration of 10 mg/L of the dye solution. However, as the concentration of the dye increased from 10 to 50 mg/L, the degradation efficiency decreased to 76.6 %. The reduced efficiency at higher dye concentrations is due to dye molecules adsorbing and hindering the incident light. This reduces the amount of light reaching the catalyst surface, decreases hole and hydroxyl radical generation, and diminishes the catalytic reaction's efficiency [81]. The effect of degradation time on EBT dye removal was evaluated over a range of 30 to 150 min. As illustrated in Fig. 10d, the degradation efficiency increased steadily with time, with the highest degradation percentage of 90 % observed at 150 min. Conversely, the lowest degradation efficiency occurred at 30 min, highlighting the time-dependent nature of the photodegradation process. This trend can be attributed to the prolonged interaction between the dye molecules and the photocatalyst, which enhances the generation and utilization of reactive species such as hydroxyl radicals (·OH) and photogenerated holes [83]. Over time, these reactive species effectively break down the

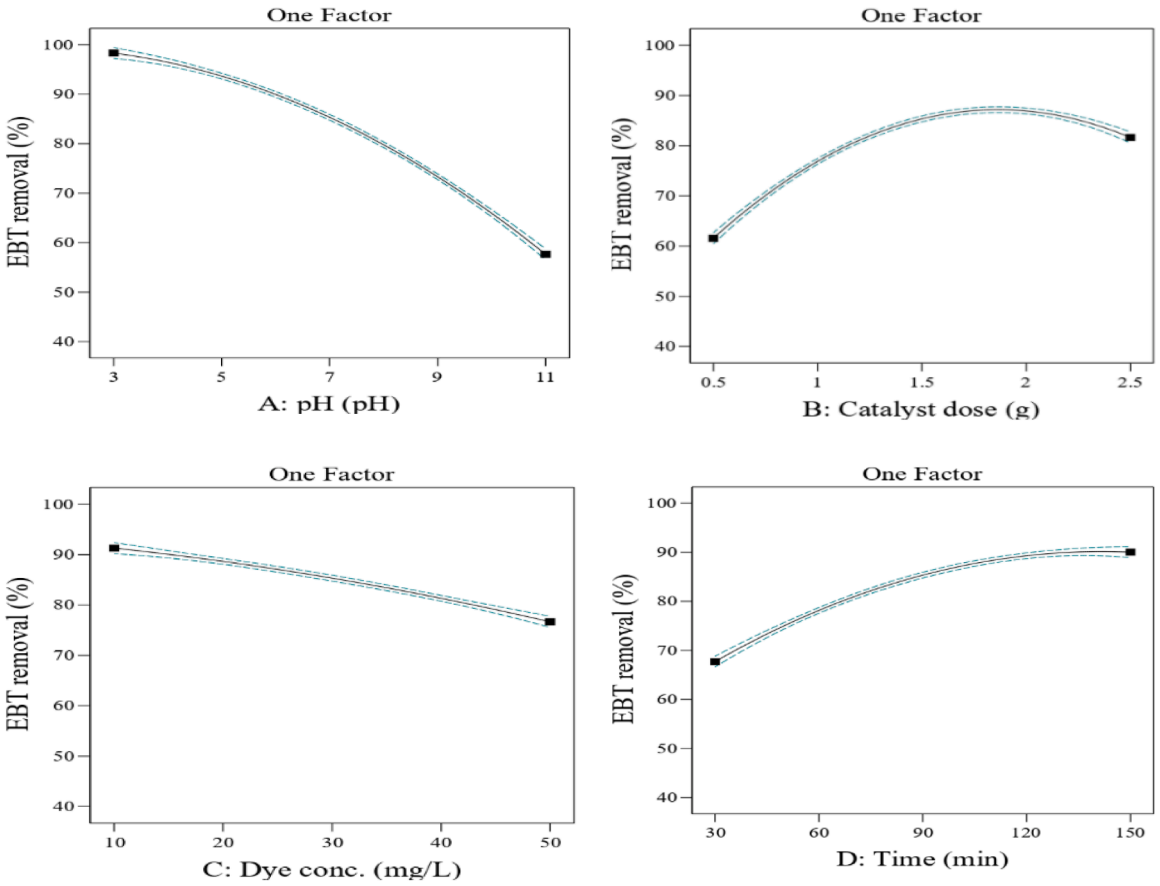

Fig. 11. Individual factor effect for degradation of EBT dye.

dye molecules, targeting chromophoric groups and azo bonds [81]. The increase in degradation efficiency with extended reaction time underscores the importance of sufficient exposure duration for maximizing photocatalytic activity. However, after a certain point, the reaction may reach saturation, where all available dye molecules are degraded or active sites become less accessible, emphasizing the need to optimize reaction time for efficient dye removal [83].

3.5. The interaction effect of factors on the degradation rate of EBT dye

3.5.1. pH and the catalyst dose

The interaction between solution pH and catalyst dosage plays a crucial role in degradation efficiency, as illustrated in Fig. 12, using both 3D and contour plots. This study explored pH levels ranging from 3 to 11 and catalyst dosages from 0.5 to 2.5 g/L, with a fixed dye concentration

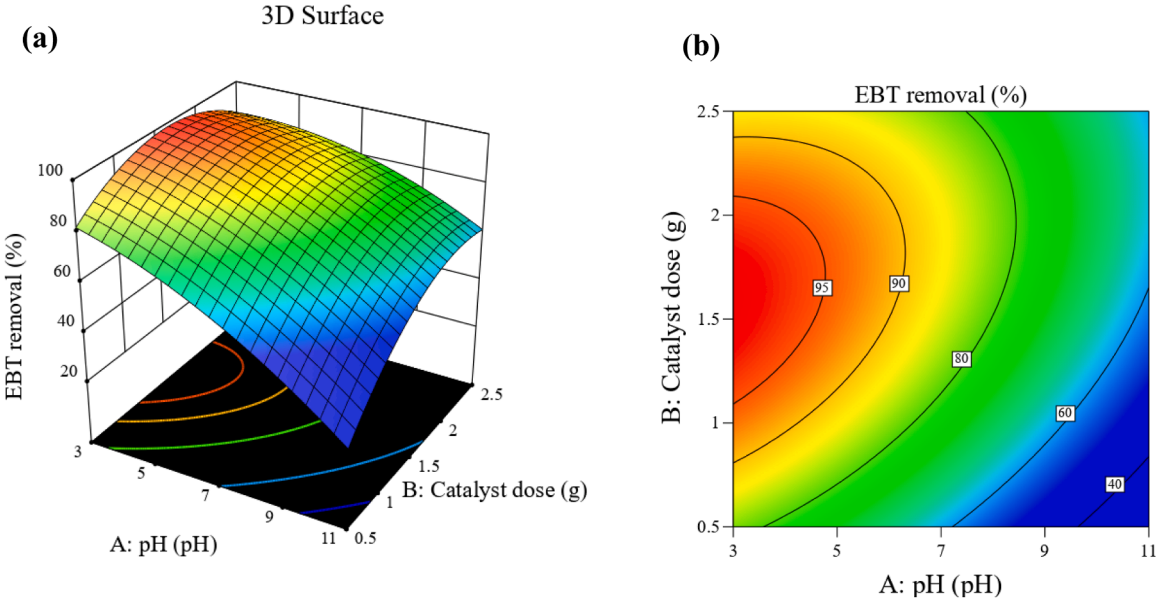

Fig. 12. 3D surface plot (a) and contour plot (b) for the interaction effect of pH and catalyst dose on the degradation efficiency of TBC-1 for EBT dye.

of 30 mg/L and a contact time of 90 min. The findings indicate that this interaction significantly enhances the degradation of BB41, with maximum efficiency (95 %) achieved at pH levels of 3 to 4 and a catalyst dosage of 1.2 to 2.2 g/L. In contrast, the lowest efficiency (~50 %) was observed at pH levels of 9 to 11 with a catalyst dose of 0.5 g/L. The analysis reveals that decreasing the pH and increasing the catalyst dosage enhance EBT dye degradation. A higher catalyst dose provides more active sites and electron-hole pairs. At the same time, a lower pH improves the interaction between the catalyst surface and the anionic EBT dye, thereby enhancing degradation efficiency. This process is influenced by the point of zero charge (pHpzc) of the TiO_2-biochar composite, the point of zero charge (pHpzc) of the TBC-1 composite is 6.28. Below this pH, TBC-1′s surface charge is positive, allowing it to adsorb the anionic EBT dye through electrostatic attraction, enhancing mass transfer and photocatalytic degradation [75]. Increasing the catalyst dosage also expands the available surface area, further improving dye removal. Lowering the pH from 11 to 3 reduces the necessary catalyst dosage while increasing the catalyst dosage shifts the optimal pH towards a more neutral range. This balance allows for more efficient catalyst use, enabling operation over a broader pH range and minimizing excessive catalyst consumption.

3.5.2. pH and initial dye concentration

The interaction effects of pH and initial dye concentration on EBT degradation, as shown in Fig. 13, reveal a clear and significant correlation, depicted through 3D surface and contour plots. The study explored a pH range of 3 to 11 and initial dye concentrations from 10 and 50 mg/L while maintaining a constant catalyst dosage of 1.5 g/L and a reaction time of 90 min. The results indicate that both pH and initial dye concentration play a crucial role in degradation efficiency. A peak degradation efficiency of over 95 % was observed at lower pH values, particularly between 3 and 6.3, and with dye concentrations between 10 and 35 mg/L. Beyond these ranges, the degradation efficiency declined, with the lowest efficiency (~63 %) recorded at a pH of 11 and higher dye concentrations (35–50 mg/L). This trend can be related to the surface charge characteristics of the TiO_2-biochar composite catalyst. At pH levels below 6.86, the TBC-1 composite acquires a positive surface charge, This enhances the adsorption of the anionic EBT dye because of electrostatic attraction [75]. Moreover, the acidic environment favors the generation of reactive species, such as holes (h+), which promote the breakdown of dye molecules [77]. Therefore, a highly acidic medium (pH < 6.3) facilitates enhanced degradation by both adsorption and photocatalytic oxidation. Conversely, as pH and dye concentration increase, degradation efficiency decreases. At elevated pH values, the surface of the TBC-1 composite develops a positive surface charge, limiting its attraction to the anionic dye. Additionally, higher dye concentrations may saturate the catalyst's active sites, leading to a reduction in overall photocatalytic activity. Optimizing both the pH and initial dye concentration provides a strategic means to enhance the photocatalytic degradation process. Operating within an acidic to neutral pH range (3–6.3) and maintaining moderate dye concentrations (10–35 mg/L) enables effective dye degradation, ensuring high efficiency and adaptability across various wastewater conditions.

3.5.3. pH and degradation time

The interaction between pH and reaction time on the removal of EBT dye, as depicted in Fig. 14, reveals a strong correlation, with the study examining pH values ranging from 3 to 11 and reaction times between 30 and 150 min, while keeping the catalyst dosage constant at 1.5 g/L and the initial dye concentration at 30 mg/L. The findings indicate that the maximum degradation efficiency (>95 %) was attained at a pH range of 3–5.5 and a reaction time of 70–120 min, whereas the lowest efficiency (~50 %) occurred at a pH range of 9–11 with a reaction time of 30 min. As the pH rose from 3 to 5.5, the required degradation time increased from 70 to 120 min, a trend linked to the surface charge properties of the TiO_2-biochar composite catalyst. At pH levels below 6.86, the catalyst exhibits a positive surface charge, enhancing the adsorption of the anionic EBT dye through electrostatic attraction [75], while the acidic conditions favor the generation of reactive species, such as holes (h+), which expedite dye degradation [77]. Thus, a highly acidic medium (pH < 6.3) facilitates more efficient degradation. Moreover, prolonged reaction times promote the formation of additional reactive radicals, further increasing the degradation process [83]. By adjusting pH and degradation time, better control over catalyst degradation can be achieved, allowing operation across a wider range of solution pH values and ensuring efficient use of degradation time.

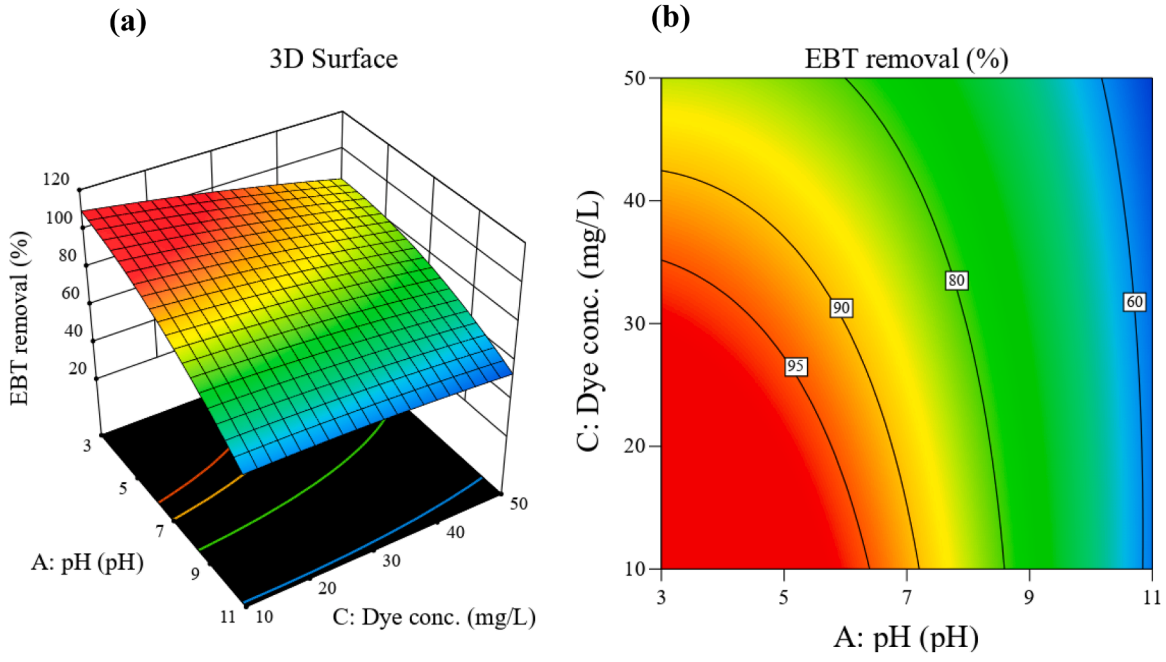

Fig. 13. 3D surface plot (a) and contour plot (b) for the interaction effect of pH and initial concentration on the degradation efficiency of TBC-1 for EBT dye.

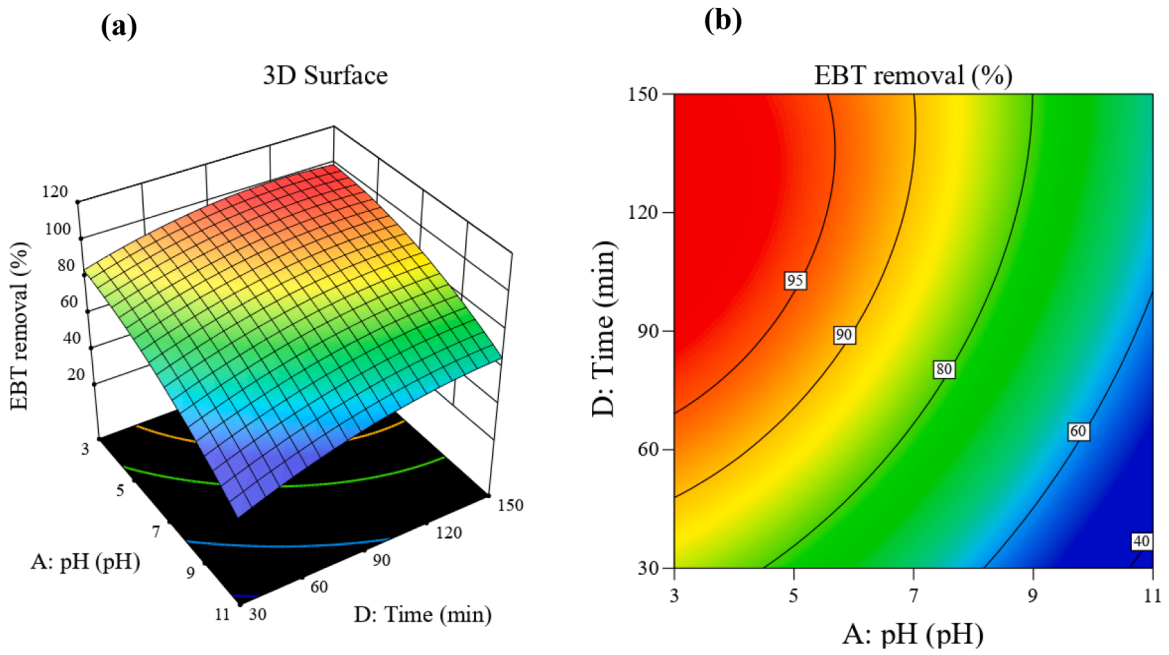

Fig. 14. 3D surface plot (a) and contour plot (b) for the interaction effect of pH and time on the degradation efficiency of TBC-1 for EBT dye.

3.5.4. Catalyst dosage and degradation time

The interaction between catalyst dosage and degradation time in the degradation of EBT dye, as shown in Fig. 15, reveals a strong correlation, supported by three-dimensional surface and contour plots. This study evaluated the catalyst dose from 0.5 to 2.5 g/L and degradation times from 30 to 150 min while maintaining a constant pH of 7 and an initial dye concentration of 30 mg/L. The result indicates that the highest degradation efficiency (90 %) was achieved with a catalyst dose between 1.5 and 2.0 g/L and reaction times of 120 to 150 min. Conversely, the lowest degradation efficiency was recorded at lower catalyst dosages (0.5–1.0 g/L) and shorter reaction times (30–70 min). This pattern illustrates the significant impact of catalyst dosage and reaction time on the photocatalytic degradation process. Increasing the photocatalyst dosage increases the number of active sites, thereby boosting the generation of reactive oxygen species necessary for degrading EBT dye molecules. Furthermore, extending the degradation time allows for prolonged exposure of the catalyst to light, which in turn facilitates the continuous production of reactive species, further enhancing the degradation efficiency [75,83]. The combined effect of increasing both the catalyst dosage and reaction time creates optimal conditions for maximum photocatalytic performance. At lower catalyst dosages (0.5–1.0 g/L) and shorter degradation times (30–70 min), the degradation efficiency significantly declines. This is likely attributed to the limited number of active sites, which restricts the generation of reactive species, combined with insufficient exposure time for adequate radical formation. The reduced number of active sites at low catalyst dosages leads to a slower reaction rate, as fewer dye molecules can be adsorbed and degraded simultaneously. Moreover, shorter reaction times do not

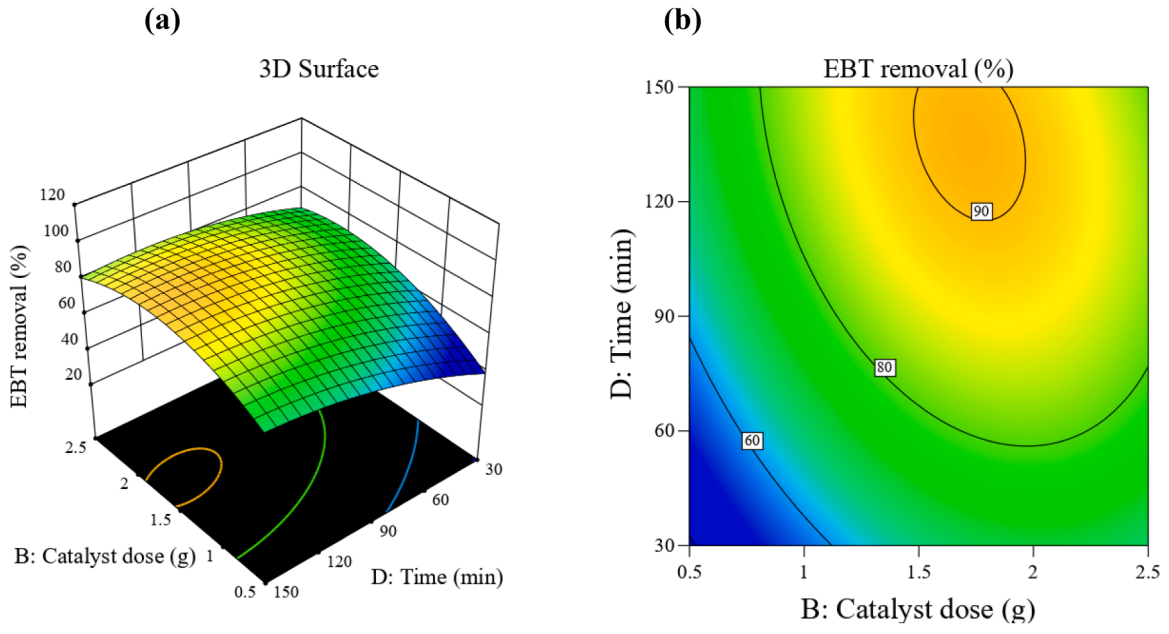

Fig. 15. 3D surface plot(a) and contour plot (b) for the interaction effect of catalyst dose and time on the degradation efficiency of TBC-1 for EBT dye.

provide enough for the formation of reactive oxygen species to achieve effective degradation performance. Overall, the study demonstrates that both catalyst dosage and reaction time play a crucial role in optimizing the degradation efficiency of EBT dye. While increasing both parameters individually can improve photocatalytic performance, their combined optimization is essential for achieving maximum efficiency. Higher catalyst dosages provide more active sites, enhancing the generation of reactive species, while extended reaction times allow for prolonged radical formation, ensuring comprehensive dye degradation.

3.6. Numerical parameter optimization

The degradation performance of the TBC-1 photocatalyst in the degradation of EBT dye was significantly enhanced through numerical optimization conducted using Design-Expert software. Key parameters such as pH (ranging from 3 to 11), catalyst dose (0.5 to 2.5 g/L), initial dye concentration (10 to 50 mg/L), and reaction time (30 to 150 min) were methodically adjusted within their specified ranges. The primary goal was to optimize color removal with a targeted confidence level of 95 %. The desirability function method was utilized to identify the optimal conditions, as shown in Fig. 16. Out of 81 potential solution sets, the most favorable configuration, achieving a desirability score of 90.6 %, was chosen. These optimal parameters involved a pH of 3.0, a catalyst dose of 1.48 g/L, an initial dye concentration of 32 mg/L, and a reaction time of 124 min, resulting in a color removal efficiency of 99.12 %. The optimization strategy achieved a 99.14 % color removal efficiency under optimal conditions, with experimental results deviating by less than 1 % from predictions, confirming the model's reliability. Additionally, a mineralization efficiency of 93.7 % highlights the catalyst's effectiveness, ensuring precision and cost-efficiency in water treatment applications. Previous studies have consistently highlighted the economic efficiency and precision of Response Surface Methodology (RSM) in experimental optimization [38,84]. The photocatalytic degradation efficiency of TiO_2-based and composite catalysts for Eriochrome Black T (EBT) removal was assessed under diverse conditions, as summarized in Table 4. The TiO_2-biochar (TBC-1) composite achieved a remarkable degradation efficiency of 99.14 %, surpassing pure TiO_2 (82 %) and advanced catalysts like N-doped TiO_2 (90 %) and TiO_2@CNTs (92 %) under UV light. Although $BaWO_4/MoS_2$ achieved a slightly higher efficiency of 99.2 % under simulated solar light, TBC-1 stands out as a more practical and sustainable alternative due to its biochar integration. Similarly, TBC-1 outperformed Ti-SBA-15 (88.7 %) under visible light conditions, showcasing superior efficiency even under UV light. The enhanced performance of TBC-1 is attributed to its biochar

Table 4
Comparison of the photocatalytic degradation efficiency of EBT dye by different catalysts.

No.	Catalyst	Condition	Degradation efficiency (%)	reference
1	TiO_2	EBT [Dye]= 25 mg/ Catalyst dosage = 0.25 g/L, for 90 min, Uv light	82 %	[10]
2	$BaWO_4/MoS_2$ Composite	EBT [Dye]=25.7mg/L, catalyst dosage = 0.25 g for 60 min, under simulated solar	99.20 %	[85]
3	N-doped TiO_2 (N-TiO_2)	EBT [dye]=100 mg/L, catalyst dosage = 3 g/ l, for 180 min under Uv light	90 %	[86]
4	titanium-modified mesoporous silica (Ti-SBA-15)	EBT [Dye]= 50 mg/L, Catalyst dosage = 3 g/ L for 70 min, under visible light irradiation	88.7 %	[87]
5	TiO_2@CNTs nanofibers	EBT [Dye]= 100 mg/L catalyst dosage= - for 100 min under UV irradiation,	92 %	[88]
6	TiO_2-BC(TBC-1)	EBT [dye] =32mg/L, pH=3 Catalyst .dosage =1.48 g/L for 124 min, under Uv light	99.14 %	This study

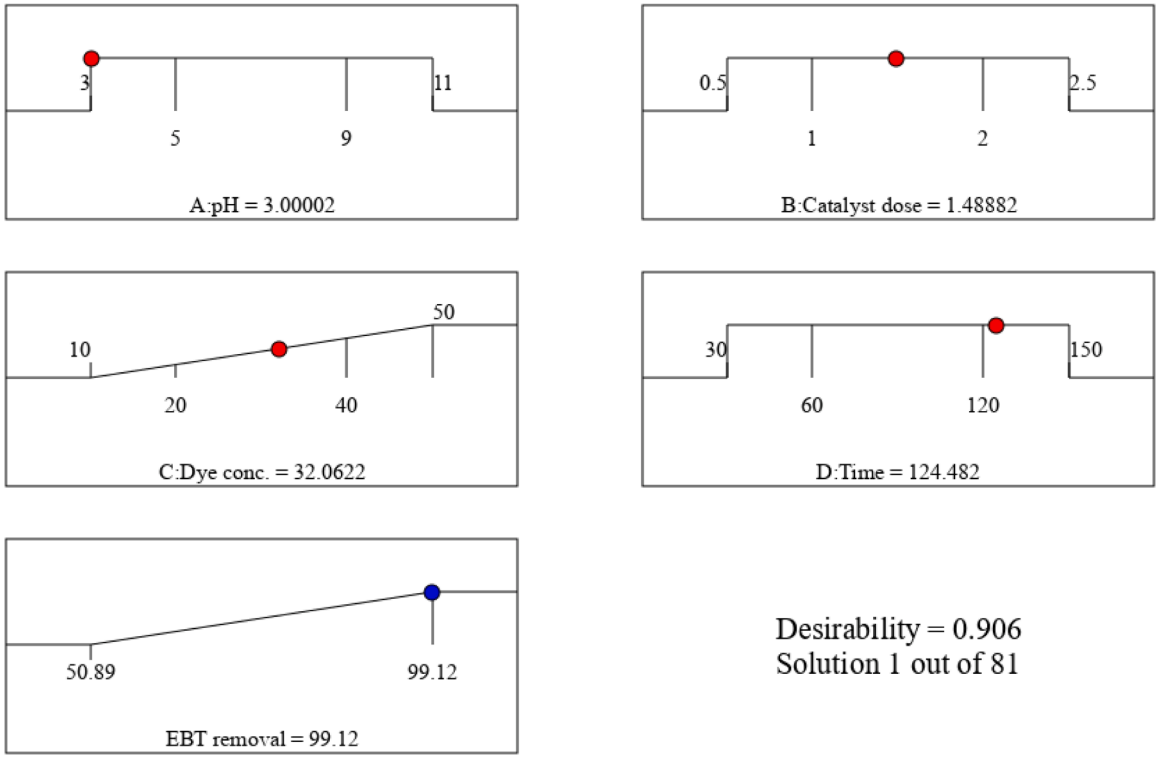

Fig. 16. Ramp plot of numerical optimized conditions for EBT dye.

component, which improves adsorption capacity, charge separation, and reactive species generation. These findings underscore TBC-1′s potential as a cost-effective, efficient, and eco-friendly catalyst for dye degradation applications.

3.7. Photodegradation kinetics

The photocatalytic degradation rates of EBT were evaluated through kinetic studies conducted under optimal conditions: pH 3.0, a catalyst dose of 1.48 g/L, an initial dye concentration of 32 mg/L, and a reaction time of 124 min. The degradation of EBT over time was modeled using first-order kinetics, with the results presented in Fig. 17. The correlation coefficients R^2 and adjusted R^2 were found to be 0.9909 and 0.989, respectively, signifying a strong model fit. The rate constant (k) was calculated as 0.051 min^{-1}, confirming that the photocatalytic degradation process adheres to first-order kinetics. The high R^2 values indicate that the first-order kinetic model effectively describes the degradation behavior of EBT. A similar study reported first-order degradation kinetics for EBT using bare anatase TiO_2 and rutile TiO_2, with rate constants of 0.058 min^{-1} and 0.056 min^{-1}, respectively [89]. Another study also reported 0.017/min using anatase TiO_2. The current study's rate constant of 0.051 /min suggests a rapid degradation of EBT under the specified conditions, aligning with the findings from the previous research.

3.8. Photocatalytic degradation mechanism

The experiments focused on trapping radicals and holes during the photocatalytic degradation of EBT dye to investigate the mechanism of pollutant degradation on the TBC-1 composite. Sodium oxalate (Na-Oxa), a typical hole scavenger, n-butanol (n-But), a hydroxyl radical scavenger, and ascorbic acid (As-Acid), a superoxide scavenger, were introduced into the EBT dye solution [47]. The results shown in Fig. 18 indicate that the photocatalytic efficiency of the TBC-1 composites with scavengers was reduced compared to the control group. The degradation of EBT dye decreased by 4.6 %, 21.6 %, and 15.8 % with the addition of scavengers As-Acid, Na-Oxa, and n-But, respectively. These findings suggest that the degradation of EBT dye was primarily influenced by holes and hydroxyl radicals, while superoxide radicals had a less significant impact. Holes, as highly reactive oxidizing agents, play a crucial role in the degradation of organic compounds, including anionic dyes, by disrupting the conjugated structures responsible for color. Research

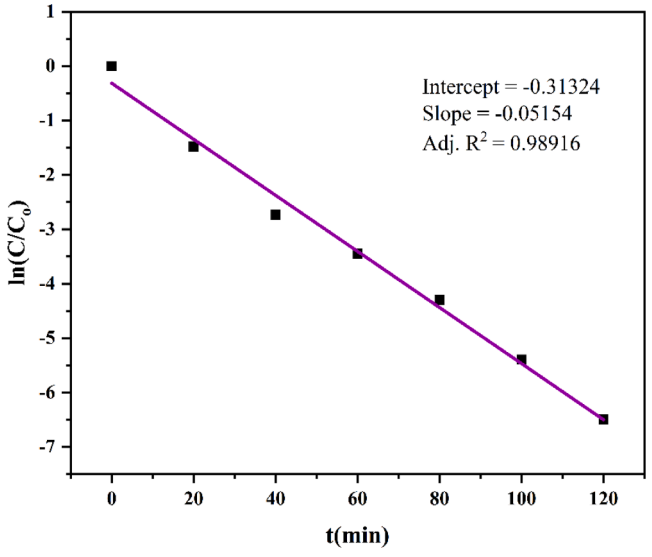

Fig. 17. First-order Kinetics of EBT dye degradation for the optimized parameter.

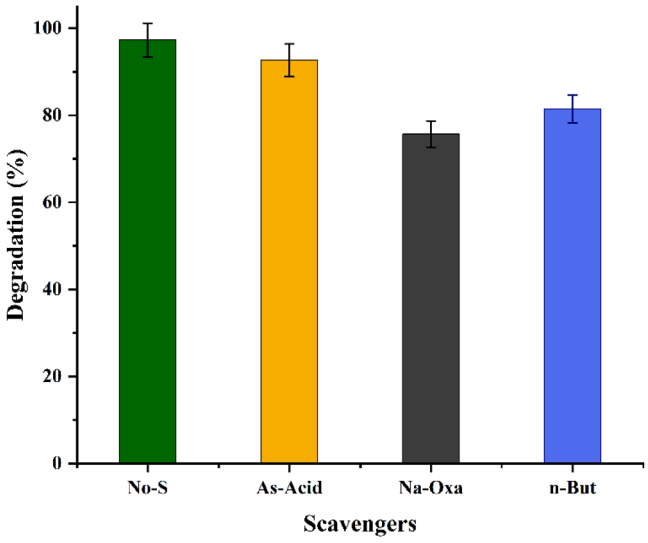

Fig. 18. Scavenger test of TBC-1 composite for EBT dye.

indicates that holes generated in photocatalytic systems account for up to 60 % of dye degradation [90]. Through oxidation of chemical bonds, holes break down complex dye structures, leading to decolorization and mineralization. Their strong oxidative capability and direct interaction with dye molecules make holes particularly effective in degrading these pollutants in environmental applications. It was concluded that holes (h+) and hydroxyl radicals (·OH) are crucial active species in the degradation process of EBT dye, with holes being the primary active species driving the degradation. The degradation mechanism of EBT dye is presented in Fig. 19.

3.9. Reusability test analysis

In this investigation, a TiO_2-biochar composite was subjected to recycling under optimal parameters, as depicted in Fig. 20. The optimized parameters for the TBC-1 photocatalyst composite included a pH of 3.0, an initial dye concentration of 32 mg/L, a catalyst dosage of 1.48 g/L, and a reaction time of 124 min. The composite underwent UV irradiation for five cycles. The findings, represented in Fig. 20, revealed that the degradation efficiency of the TBC-1 composite remained significantly high at the outset. Following the fourth recycling iteration, a marginal decline in degradation efficiency for the EBT dye was observed. Throughout the five recycling cycles, the degradation

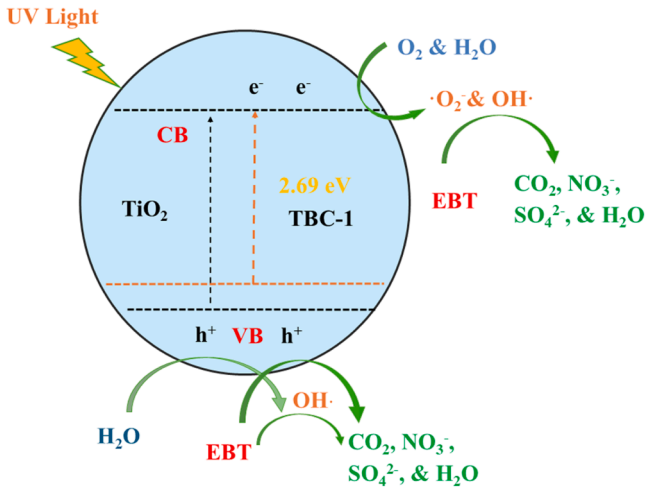

Fig. 19. The schematic diagram for EBT degradation via TBC-1 photocatalysis.

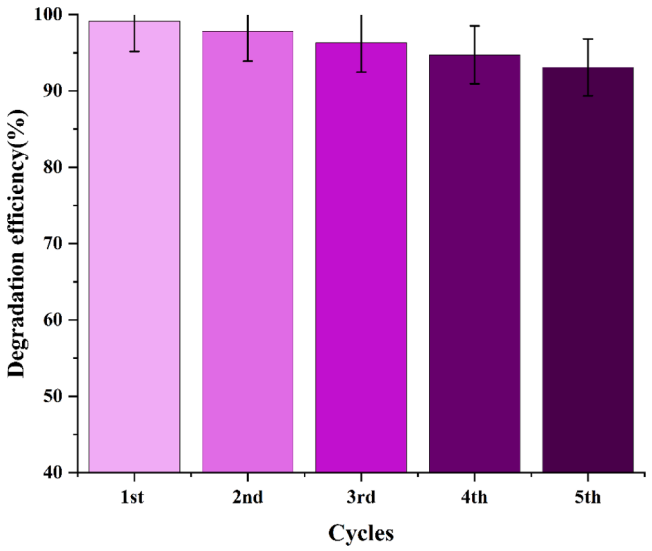

Fig. 20. Recycling test of TBC-1 composite for EBT dye.

efficiency diminished from 99.14 % to 93.09 %, indicating a reduction of merely 6.05 %. This shows the composite catalyst's ability to sustain elevated photodegradation efficiency and confirms the TBC-1 catalyst's remarkable efficacy in degrading EBT dye. Moreover, the recycling process does not require any additional treatment, indicating the catalyst's potential as a practical and feasible solution for water treatment.

4. Conclusion

In summary, the TBC-1 composite photocatalyst was successfully synthesized via the Sol-Gel method at 600 °C, resulting in an anatase crystal structure. This resulted in a reduced band gap of 2.69 eV and an increase in surface area from 38 m^2/g to 78 m^2/g. The photocatalytic efficiency was optimized using RSM with CCD under UV irradiation. The ANOVA confirmed the high significance of the color removal model ($p < 0.05$) with an R^2 value of 0.998. The key factors influencing the process included initial pH (3–11), photocatalyst dosage (0.5–2.5 g/L), dye concentration (10–50 mg/L), and irradiation time (30–150 min). The photodegradation of EBT dye under optimal conditions of pH 3, 32 mg/L dye concentration, 1.48 g/L catalyst dosage, and 124 min of irradiation resulted in 99.14 % decolorization efficiency and 93.7 % mineralization efficiency, demonstrating the process's effectiveness. The dye degradation followed first-order kinetics with a rate constant of $k = 0.051\ min^{-1}$. Remarkably, the composite maintained its photocatalytic performance over five recycling cycles, with only a 6.05 % reduction in efficiency. Thus, the TBC-1 composite photocatalyst offers a promising, cost-effective, and eco-friendly solution for dye pollutant removal from aqueous systems.

5. Funding

The research was conducted at Addis Ababa Science and Technology University and was not funded. There was no financial support for the manuscript writing or editing approval.

CRediT authorship contribution statement

Mohammednur Abdu: Writing – review & editing, Writing – original draft, Visualization, Validation, Software, Methodology, Investigation, Formal analysis, Data curation, Conceptualization. **Solomon Tibebu:** Visualization, Validation, Formal analysis. **Saeideh Babaee:** Visualization, Validation, Formal analysis. **Abebe Worku:** Writing – original draft, Visualization, Validation, Software, Methodology, Investigation, Formal analysis, Data curation, Conceptualization. **Titus A.M. Msagati:** Writing – review & editing, Writing – original draft, Visualization, Validation, Supervision, Software, Methodology, Investigation, Formal analysis, Data curation, Conceptualization. **Jemal Fito Nure:** Writing – review & editing, Writing – original draft, Visualization, Validation, Software, Methodology, Investigation, Formal analysis, Data curation, Conceptualization.

Declaration of competing interest

The authors declare that they have no known competing financial interests or personal relationships that could have appeared to influence the work reported in this paper.

Acknowledgments

We would like to thank Addis Ababa Science and Technology University for its support.

Data availability

Data will be made available on request.

References

[1] A Arif, M Malik, S Liaqat, A Aslam, K Mumtaz, A Afzal, et al., Water pollution and industries, Pure Appl. Biol. 9 (4) (2020) 2214–2224.
[2] S Ahmed, Ismail S %J SA, pollution SI 'Water, its sources e, management: a case study of Delhi' IJ of CAR, Water Pollution and its Sources, Effects Manag.: A Case Study of Delhi 7 (2) (2018) 10436–10442.
[3] Doetterl S, Van Oost K, Six J %J ESP, Landforms. Towards constraining the magnitude of global agricultural sediment and soil organic carbon fluxes. 2012;37 (6):642–55.
[4] ML Serejo, MF Morgado, D García, A González-Sánchez, Méndez-Acosta HO, A. Toledo-Cervantes, Environmental resilience by microalgae, in: Microalgae Cultivation for Biofuels Production, Elsevier, 2020, pp. 293–315.
[5] Cui J, Zhang F, Li H, Cui J, Ren Y, Yu X %J AS. Recent progress in biochar-based photocatalysts for wastewater treatment: synthesis, mechanisms, and applications. 2020;10(3):1019.
[6] Kittappa S, Jais FM, Ramalingam M, Mohd NS, Ibrahim S %J J of ECE. Functionalized magnetic mesoporous palm shell activated carbon for enhanced removal of azo dyes. 2020;8(5):104081.
[7] R Mansour, %J H of renewable materials for coloration, finishing, Natural Dyes and Pigments: Extract. Appl (2018) 75–102.
[8] S Ariaeenejad, K Kavousi, M Zeinalabedini, D Afshar Jahanshahi, SR Beh-Afarin, Enhanced bioremediation of saline azo dye effluents using PersiLac3: A thermo-halotolerant laccase from a tannery metagenome, Results Eng. [Internet] 24 (2024) 103172. Available from, https://www.sciencedirect.com/science/article/pii/S2590123024014270.
[9] M Hosseini, M Ghanbari, EA Dawi, MH Shuhata Alubiady, AM Al-Ani, AF Alkaim, et al., $CaSnO_3$/g-C_3N_4 S-scheme heterojunction photocatalyst for the elimination of erythrosine and eriochrome black T from water under visible light, Results Eng. [Internet] 21 (2024) 101903. Available from, https://www.sciencedirect.com/science/article/pii/S2590123024001567.
[10] SK Kansal, S Sood, A Umar, SK. Mehta, Photocatalytic degradation of Eriochrome Black T dye using well-crystalline anatase TiO_2 nanoparticles, J. Alloys Compd. 581 (2013) 392–397.
[11] DA Yaseen, Scholz M %J I journal of environmental science, technology, Textile dye wastewater characteristics and constituents of synthetic effluents: a critical review 16 (2) (2019) 1193–1226.
[12] Modirshahla N, Hassani A, Behnajady MA, Rahbarfam R %J D. Effect of operational parameters on decolorization of Acid Yellow 23 from wastewater by UV irradiation using ZnO and ZnO/SnO2 photocatalysts. 2011;271(1–3):187–92.
[13] SS Hutagalung, I Muchlis, K. Khotimah, Textile wastewater treatment using advanced oxidation process (AOP), in: IOP conference series: materials science and engineering, IOP Publishing, 2020, p. 12032.
[14] Yao C, Wang M, Jiang W, Chen Y %J EER. Study on a novel N-doped mesoporous carbon for the efficient removal of methylene blue from aqueous solution. 2021;26 (5).
[15] Ameta Udaipur, Rajasthan, India SC %J EGCTPU. Introduction, In: Advanced Oxidation Processes for Waste Water Treatment. 2018;1–12.
[16] AA Aziz, S Ibrahim, Preparation of activated carbon/N-doped titania composite for synergistic adsorption-photocatalytic oxidation of batik dye, in: IOP Conference Series: Materials Science and Engineering, IOP Publishing, 2018, p. 12014.
[17] Plakas K V, Taxintari A, Karabelas AJ %J W. Enhanced Photo-Catalytic Performance of Activated Carbon Fibers for Water Treatment. 2019;11(9):1794.
[18] N Madkhali, C Prasad, K Malkappa, HY Choi, V Govinda, I Bahadur, et al., Recent update on photocatalytic degradation of pollutants in wastewater using TiO_2-based

heterostructured materials, Results Eng. [Internet] 17 (2023) 100920. Available from, https://www.sciencedirect.com/science/article/pii/S2590123023000476.
[19] J Zhou, B Zhu, L Wang, Y Li, Q. Qiao, Enhanced photocatalytic activity of Fe-doped TiO_2 coated on N-doped activated carbon composites for photocatalytic degradation of dyeing wastewater, in: AIP Conference Proceedings, AIP Publishing LLC, 2017, p. 20009.
[20] Khlyustova A, Sirotkin N, Kusova T, Kraev A, Titov V, Agafonov A %J MA. Doped TiO2: the effect of doping elements on photocatalytic activity. 2020;1(5): 1193–201.
[21] Yalçın Y, Kılıç M, Çınar Z %J J of AOT. The role of non-metal doping in TiO2 photocatalysis. 2010;13(3):281–96.
[22] Fazal T, Razzaq A, Javed F, Hafeez A, Rashid N, Amjad US, et al. Integrating adsorption and photocatalysis: a cost effective strategy for textile wastewater treatment using hybrid biochar-TiO2 composite. 2020;390:121623.
[23] Adnan MAM, Julkapli NM, Amir MNI, Maamor A %J IJ of ES, Technology. Effect on different TiO2 photocatalyst supports on photodecolorization of synthetic dyes: a review. 2019;16(1):547–66.
[24] NAM Barakat, HA Omran, MK Hassan, AF Mohamed, AH Backar, OM Irfan, et al., Graphite-TiO_2-doped coated sand granules for efficient continuous removal of methylene blue dye: Combining adsorption and photocatalytic degradation, Results Eng. [Internet] 20 (2023) 101646. Available from, https://www.sciencedirect.com/science/article/pii/S2590123023007739.
[25] Ghosh T, Oh W %J AJ of C. Carbon based titania photocatalysts. 2012;24(12): 5419–23.
[26] L Lu, R Shan, Y Shi, S Wang, H. Yuan, Chemosphere A novel TiO_2 /biochar composite catalysts for photocatalytic degradation of methyl orange, Chemosphere [Internet] 222 (2019) 391–398, https://doi.org/10.1016/j.chemosphere.2019.01.132. Available from.
[27] Xiong X, Iris KM, Cao L, Tsang DCW, Zhang S, Ok YS %J B technology. A review of biochar-based catalysts for chemical synthesis, biofuel production, and pollution control. 2017;246:254–70.
[28] L Wang, J Ali, Z Wang, NA Oladoja, R Cheng, C Zhang, et al., Oxygen nanobubbles enhanced photodegradation of oxytetracycline under visible light: Synergistic effect and mechanism, Chem. Eng. J. [Internet] 388 (2020) 124227. Available from, https://www.sciencedirect.com/science/article/pii/S1385894720302187.
[29] Liu WJ, Jiang H, Yu HQ %J C reviews. Development of biochar-based functional materials: toward a sustainable platform carbon material. 2015;115(22): 12251–85.
[30] Zhang H, Wang Z, Li R, Guo J, Li Y, Zhu J, et al. TiO2 supported on reed straw biochar as an adsorptive and photocatalytic composite for the efficient degradation of sulfamethoxazole in aqueous matrices. 2017;185:351–60.
[31] Silvestri S, Goncalves MG, da Silva Veiga PA, da Silva Matos TT, Peralta-Zamora P, Mangrich AS %J J of ECE. TiO2 supported on Salvinia molesta biochar for heterogeneous photocatalytic degradation of Acid Orange 7 dye. 2019;7(1): 102879.
[32] Wang B, Liu B, Ji XX, Ma MG %J M. Synthesis, characterization, and photocatalytic properties of bamboo charcoal/TiO2 composites using four sizes powder. 2018;11 (5):670.
[33] Zhang S, Lu X %J C. Treatment of wastewater containing Reactive Brilliant Blue KN-R using TiO2/BC composite as heterogeneous photocatalyst and adsorbent. 2018;206:777–83.
[34] Kim JR, Kan E %J J of environmental management. Heterogeneous photocatalytic degradation of sulfamethoxazole in water using a biochar-supported TiO2 photocatalyst. 2016;180:94–101.
[35] Cai X, Li J, Liu Y, Yan Z, Tan X, Liu S, et al. Titanium dioxide-coated biochar composites as adsorptive and photocatalytic degradation materials for the removal of aqueous organic pollutants. 2018;93(3):783–91.
[36] Lansdown R V, Knees SG, Patzelt A. Bacopa monnieri. The IUCN Red list of Threatened Species 2013: e. T164168A17722668. 2013.
[37] Y Zhao, L Huang, Y. Chen, Biochars derived from giant reed (Arundo donax L.) with different treatment: characterization and ammonium adsorption potential, Environ. Sci. Pollution Res. 24 (2017) 25889–25898.
[38] E Kweinor Tetteh, E Obotey Ezugbe, D Asante-Sackey, EK Armah, S Rathilal, Response surface methodology: photocatalytic degradation kinetics of basic blue 41 dye using activated carbon with TiO_2, Molecules [Internet] 26 (4) (2021). Available from, https://www.mdpi.com/1420-3049/26/4/1068.
[39] S Hmamouchi, A El Yacoubi, M El Hezzat, B Sallek, BC El Idrissi, Optimization of photocatalytic parameters for MB degradation by g-C_3N_4 nanoparticles using Response Surface Methodology (RSM), Diamond Relat. Mater. [Internet] 136 (2023) 109986. Available from, https://www.sciencedirect.com/science/article/pii/S0925963523003114.
[40] M Hasanpour, S Motahari, D Jing, M. Hatami, Statistical analysis and optimization of photodegradation efficiency of methyl orange from aqueous solution using cellulose/zinc oxide hybrid aerogel by response surface methodology (RSM), Arabian J. Chem. [Internet] 14 (11) (2021) 103401. Available from, https://www.sciencedirect.com/science/article/pii/S1878535221004160.
[41] SJS Chelladurai, K Murugan, AP Ray, M Upadhyaya, V Narasimharaj, S. Gnanasekaran, Optimization of process parameters using response surface methodology: A review, Mater. Today: Proc. 37 (2021) 1301–1304.
[42] M Abdu, S Babaee, A Worku, TAM Msagati, JF. Nure, The development of giant reed biochar for adsorption of basic blue 41 and Eriochrome Black T. azo dyes from wastewater, Scientific Reports [Internet] 14 (1) (2024) 18320, https://doi.org/10.1038/s41598-024-67997-5. Available from.
[43] H Elbushra, M Ahmed, H Wardi, N. Eassa, Synthesis and characterization of TiO_2 using sol-gel method at different annealing temperatures, MRS Advances [Internet] 3 (42–43) (2018) 2527–2535, 2018/02/26Available from, https://www.cambridge.org/core/product/E2A2D89C9972E5165503BB8D9D61C428.
[44] Y Jiang, A. Liu, Cornstalk biochar-TiO_2 composites as alternative photocatalyst for degrading methyl orange, Environ. Sci. Pollution Res. 30 (11) (2023) 31923–31934.
[45] T Mahmood, MT Saddique, A Naeem, P Westerhoff, S Mustafa, A. Alum, Comparison of different methods for the point of zero charge determination of NiO, Indust. Eng. Chem. Res. [Internet] 50 (17) (2011 Sep 7) 10017–10023, https://doi.org/10.1021/ie200271d. Available from.
[46] N Rosly, A Abdullah, M Ahmad Kamarudin, E Ashari, S Ahmad, Adsorption of methylene blue dye by Calix[6]Arene-modified lead sulphide (Pbs): optimisation using response surface methodology, Int. J. Environ. Res. Public Health 18 (2021) 397.
[47] B Mondol, A Sarker, AM Shareque, SC Dey, MT Islam, AK Das, et al., Preparation of activated carbon/TiO_2 nanohybrids for photodegradation of reactive red-35 dye using sunlight, Photochem 1 (1) (2021) 54–66.
[48] MM El Bouraie, SS Ibrahim, Comparative study between metronidazole residues disposal by using adsorption and photodegradation processes onto MgO nanoparticles, J. Inorg. Organomet. Polym. Mater. 31 (1) (2021) 344–364.
[49] Y Yan, S Manickam, E Lester, T Wu, CH. Pang, Synthesis of graphene oxide and graphene quantum dots from miscanthus via ultrasound-assisted mechano-chemical cracking method, Ultrason. Sonochem. (2021) 73.
[50] AC Martins, AL Cazetta, O Pezoti, JRB Souza, T Zhang, EJ Pilau, et al., Sol-gel synthesis of new TiO2/activated carbon photocatalyst and its application for degradation of tetracycline, Ceram. Int. 43 (5) (2017) 4411–4418.
[51] R Wu, W Liu, R Bai, D Zheng, X Tian, W Lin, et al., Waste biomass-mediated synthesis of TiO_2/P, K-containing grapefruit peel biochar composites with enhanced photocatalytic activity, Molecules 29 (9) (2024) 2090.
[52] Y Liu, X Dai, J Li, S Cheng, J Zhang, Y. Ma, Recent progress in TiO_2–biochar-based photocatalysts for water contaminants treatment: strategies to improve photocatalytic performance, RSC Adv. 14 (1) (2024) 478–491.
[53] AK Singh, DA Giannakoudakis, M Arkas, KS Triantafyllidis, V. Nair, Composites of lignin-based biochar with BiOCl for photocatalytic water treatment: RSM studies for process optimization, Nanomaterials [Internet] 13 (4) (2023). Available from, https://www.mdpi.com/2079-4991/13/4/735.
[54] J Wang, T Yu, M Wang, X Guo, Y. Chen, A novel biochar-composed TiO_2 (BC-Ti) for efficient photocatalytic degradation on arbidol, J. Ind. Eng. Chem. 134 (2024) 537–547.
[55] MA Gatou, A Syrrakou, N Lagopati, EA. Pavlatou, Photocatalytic TiO_2-based nanostructures as a promising material for diverse environmental applications: a review, Reactions 5 (1) (2024) 135–194.
[56] AK Inamdar, SA Inamdar, CT Birajdar, J Bhale, S V Rajmane, BH Shinde, et al., Applications of titanium dioxide (TiO_2) nanoparticles in photocatalysis, Sci. Adv. Mater. 16 (7) (2024) 757–771.
[57] Y Wei, H Meng, Q Wu, X Bai, Y. Zhang, TiO_2-based photocatalytic building material for air purification in sustainable and low-carbon cities: a review, Catalysts 13 (12) (2023) 1466.
[58] Lisowski P, Colmenares JC, Mašek O. Dual functionality of TiO2 /biochar hybrid materials : photocatalytic phenol degradation in liquid phase and selective oxidation of methanol in gas phase. 2017.
[59] E Dervishi, Z Ji, H Htoon, M Sykora, SK. Doorn, Raman spectroscopy of bottom-up synthesized graphene quantum dots: size and structure dependence, Nanoscale [Internet] 11 (35) (2019) 16571–16581, https://doi.org/10.1039/C9NR05345J. Available from.
[60] AA George, O IJ, OD. Victoria, Production of biochar from elephant grass (Pernisetum purpureum) using an updraft biomass gasifier with retort heating, Biofuels [Internet] 0 (0) (2019) 1–8, https://doi.org/10.1080/17597269.2019.1613751. Available from.
[61] E Al-Oubidy, F. Kadhim, Photocatalytic activity of anatase titanium dioxide nanostructures prepared by reactive magnetron sputtering technique, Opt. Quantum Electron. (2019 Jan 3) 51.
[62] Xing B, Shi C, Zhang C, Yi G, Chen L, Guo H, et al. Preparation of TiO2 /Activated Carbon Composites for Photocatalytic Degradation of RhB under UV Light Irradiation. 2016;2016.
[63] Kowalczyk A, Zgardzińska B, Osipiuk K, Jędruchniewicz K, Rotko KT, Goździuk M, et al. The Visible - Light - Driven Activity of Biochar - Doped TiO2 Photocatalysts in β - Blockers Removal from Water. 2023.
[64] J Song, M Shi, L Xia, J Dai, L Luo, H Wang, et al., The comparative study on inhibitory effect of natural organic matters on the TiO_2 and activated carbon/TiO_2 composites for the removal of 17α-ethinylestradiol, Chemosphere [Internet] 333 (2023) 138930. Available from, https://www.sciencedirect.com/science/article/pii/S0045653523011979.
[65] S Samangsri, Chiarakorn TAS. of methylene blue dye, Research on Chemical Intermediates [Internet] 49 (4) (2023) 1649–1664, https://doi.org/10.1007/s11164-022-04925-0. Available from.
[66] Wang W, Zhang J, Chen T, Sun J, Ma X, Wang Y, et al. Preparation of TiO2-modified Biochar and its Characteristics of Photo-catalysis Degradation for Enrofloxacin. 2020;10(1):1–12.
[67] KR Gustavsen, T Feng, H Huang, G Li, U Narkiewicz, K. Wang, DFT Calculation of Carbon-Doped TiO_2 Nanocomposites, Materials [Internet] 16 (18) (2023). Available from, https://www.mdpi.com/1996-1944/16/18/6117.
[68] K Jedynak, B. Charmas, Adsorption properties of biochars obtained by KOH activation, Adsorption [Internet] (2023), https://doi.org/10.1007/s10450-023-00399-7. Available from.

[69] Zeng M. Influence of TiO2 surface properties on water pollution treatment and photocatalytic activity influence of TiO2 surface properties on water pollution treatment and photocatalytic activity. 2015;(November):2–6.
[70] M An, Z Yang, B Zhang, B Xue, G Xu, W Chen, et al., Construction of biochar-modified TiO_2 anatase-rutile phase S-scheme heterojunction for enhanced performance of photocatalytic degradation and photocatalytic hydrogen evolution, J. Environ. Chem. Eng. 11 (5) (2023) 110367.
[71] MS Mohtaram, S Mohtaram, S Sabbaghi, X You, W Wu, L Jia, et al., Photocatalytic degradation of acetaminophen using a novel TiO_2-orange peel-derived biochar composite: Synthesize, characterization and optimization of key factors, J. Water Process Eng. 58 (2024) 104884.
[72] S Hmamouchi, Y Abbad, A El Yacoubi, A Boulouiz, B Sallek, BC El Idrissi, Optimization study of methylene blue dye adsorption on Chamaerops humilis fibers biosorption using a central composite design, Desalination and Water Treatment [Internet] 320 (2024) 100824. Available from, https://www.sciencedirect.com/science/article/pii/S1944398624203349.
[73] H Chaker, N Ameur, K Saidi-Bendahou, M Djennas, S. Fourmentin, Modeling and Box-Behnken design optimization of photocatalytic parameters for efficient removal of dye by lanthanum-doped mesoporous TiO_2, J. Environ. Chem. Eng. 9 (1) (2021) 104584.
[74] K Sadraoui, T Ahl El Haj, K El Mejdoubi, A El Yacoubi, Y Elrhayam, M Berradi, et al., Kinetics, thermodynamics, and optimization studies using response surface methodology in quinoxalines synthesis with efficient heterogeneous catalysts: environmental sustainability metrics assessment, Res. Chem. Intermed. [Internet] (2024), https://doi.org/10.1007/s11164-024-05410-6. Available from.
[75] P Gharbani, A Mehrizad, SA. Mosavi, Optimization, kinetics and thermodynamics studies for photocatalytic degradation of Methylene Blue using cadmium selenide nanoparticles, npj Clean Water [Internet] 5 (1) (2022) 34, https://doi.org/10.1038/s41545-022-00178-x. Available from.
[76] U Fegade, G Jethave, WG Hong, I Khan, HM Marwani, Inamuddin, et al., Multifunctional Zn0.3Al0.4O4.5 crystals: An efficient photocatalyst for formaldehyde degradation and EBT adsorption, Arabian J. Chem. [Internet] 13 (11) (2020) 8262–8270. Available from, https://www.sciencedirect.com/science/article/pii/S1878535220301088.
[77] A Ajmal, I Majeed, RN Malik, H Idriss, MA. Nadeem, Principles and mechanisms of photocatalytic dye degradation on TiO_2 based photocatalysts: a comparative overview, RSC Adv. 4 (70) (2014) 37003–37026.
[78] AO Ifebajo, AA Oladipo, M. Gazi, Sun-light driven enhanced azo dye decontamination from aqueous solution by CoO− CuFe, Desalin Water Treat. 2020 177 (2020) 423–430.
[79] A. Solmaz, Adsorption of methylene blue and eriochrome black t onto pinecone powders (Pinus nigra Arn.): equilibrium, kinetics, and thermodynamic studies, Processes [Internet] 12 (9) (2024). Available from, https://www.mdpi.com/2227-9717/12/9/2044.
[80] S Charafi, FZ Janani, A Elhalil, M Abdennouri, M Sadiq, N. Barka, Adsorption and reusability performances of Ni/Al layered double hydroxide for the removal of Eriochrome Black T dye, Biointerface Res. Appl. Chem. 13 (3) (2023).
[81] KM Reza, ASW Kurny, F. Gulshan, Parameters affecting the photocatalytic degradation of dyes using TiO_2: a review, Appl. Water Sci. 7 (2017) 1569–1578.
[82] A Zuorro, R Lavecchia, MM Monaco, G Iervolino, V. Vaiano, Photocatalytic degradation of azo dye reactive violet 5 on Fe-doped titania catalysts under visible light irradiation, Catalysts 9 (8) (2019) 645.
[83] SM Anisuzzaman, CG Joseph, CK Pang, NA Affandi, SN Maruja, V. Vijayan, Current trends in the utilization of photolysis and photocatalysis treatment processes for the remediation of dye wastewater: a short review, Chem. Eng. [Internet] 6 (4) (2022). Available from, https://www.mdpi.com/2305-7084/6/4/58.
[84] S Mortazavian, A Saber, DE. James, Optimization of photocatalytic degradation of acid blue 113 and acid red 88 textile dyes in a UV-C/TiO_2 suspension system: application of response surface methodology (RSM), Catalysts 9 (4) (2019) 360.
[85] YM Hunge, AA Yadav, SW. Kang, Photocatalytic degradation of eriochrome black-T Using $BaWO_4/MoS_2$ composite, Catalysts [Internet] 12 (10) (2022). Available from, https://www.mdpi.com/2073-4344/12/10/1290.
[86] O Sacco, A Mancuso, V Venditto, S Pragliola, V. Vaiano, Behavior of N-Doped TiO_2 and N-Doped ZnO in photocatalytic azo dye degradation under UV and visible light irradiation: a preliminary investigation, Catalysts [Internet] 12 (10) (2022). Available from, https://www.mdpi.com/2073-4344/12/10/1208.
[87] HM Gobara, RA Elsalamony, SA. Hassan, Sonophotocatalytic degradation of Eriochrome black-T dye in water using Ti grafted SBA-15, J. Porous Mater. [Internet] 23 (5) (2016) 1311–1318, https://doi.org/10.1007/s10934-016-0190-3. Available from.
[88] J Zhu, Z. Jiang, Electrochemical photocatalytic degradation of eriochrome black T dye using synthesized TiO_2@CNTs nanofibers, Int. J. Elect. Sci. [Internet] 16 (3) (2021) 210318. Available from, https://www.sciencedirect.com/science/article/pii/S1452398123029231.
[89] A Gautam, A Kshirsagar, R Biswas, S Banerjee, PK. Khanna, Photodegradation of organic dyes based on anatase and rutile TiO_2 nanoparticles, RSC Adv. 6 (4) (2016) 2746–2759.
[90] L Kuang, Y Zhao, W Zhang, S. Ge, Roles of reactive oxygen species and holes in the photodegradation of cationic and anionic dyes by TiO_2 under UV irradiation, J. Environ. Eng. 142 (2) (2016) 4015065.